



Published in final edited form as:

Cell. 2018 December 13; 175(7): 1780–1795.e19. doi:10.1016/j.cell.2018.10.001.

Distinct Regulation of Th17 and Th1 Cell Differentiation by Glutaminase-Dependent Metabolism

Marc O. Johnson^{1,2}, Melissa M. Wolf¹, Matthew Z. Madden¹, Gabriela Andrejeva¹, Ayaka Sugiura¹, Diana C. Contreras¹, Damian Maseda¹, Maria V. Liberti², Katelyn Paz³, Rigel J. Kishton⁴, Matthew E. Johnson⁵, Aguirre A. de Cubas⁶, Pingsheng Wu⁷, Gongbo Li⁸, Yongliang Zhang⁸, Dawn C. Newcomb^{7,9}, Andrew D. Wells⁵, Nicholas P. Restifo⁴, W. Kimryn Rathmell^{6,9}, Jason W. Locasale², Marco L. Davila⁸, Bruce R. Blazar³, and Jeffrey C. Rathmell^{1,9,10,*}

¹Department of Pathology, Microbiology, and Immunology, Vanderbilt University Medical Center, Nashville, TN 37232, USA

²Department of Pharmacology and Cancer Biology, Duke University, Durham, NC 27710, USA

³Department of Pediatrics, University of Minnesota, Minneapolis, MN 55455, USA

⁴Center for Cell-Based Therapy, National Cancer Institute, National Institutes of Health, Bethesda, MD 20892, USA

⁵Department of Pathology and Laboratory Medicine, The Children's Hospital of Philadelphia and the Perelman School of Medicine at the University of Pennsylvania, Philadelphia, PA 19104, USA

⁶Department of Medicine, Division of Hematology and Oncology, Vanderbilt University Medical Center, Nashville, TN 37232, USA

⁷Division of Allergy, Pulmonary and Critical Care Medicine, Department of Medicine, Vanderbilt University School of Medicine, Nashville, TN 37232, USA

⁸Department of Blood and Marrow Transplantation and Cellular Immunotherapy, H. Lee Moffitt Cancer Center and Research Institute, Tampa, FL 33612, USA

⁹Vanderbilt Center for Immunobiology, Vanderbilt Institute for Infection, Immunology, and Inflammation, Vanderbilt University School of Medicine, Nashville, TN 37232, USA

¹⁰Lead Contact

SUMMARY

*Correspondence: jeff.rathmell@vumc.org.

AUTHOR CONTRIBUTIONS

M.O.J. and J.C.R. designed and oversaw the study; M.O.J., M.M.W., M.V.L., K.P., A.A.d.C., D.M., R.J.K., G.A., D.C.C., M.E.J., A.S., M.Z.M., P.W., G.L., and Y.Z. performed experiments and data analysis; A.D.W., N.P.R., J.W.L., W.K.R., D.C.N., M.L.D., and B.R.B. supervised and provided expertise in experimental design and data interpretation; M.O.J. and J.C.R. wrote the manuscript.

SUPPLEMENTAL INFORMATION

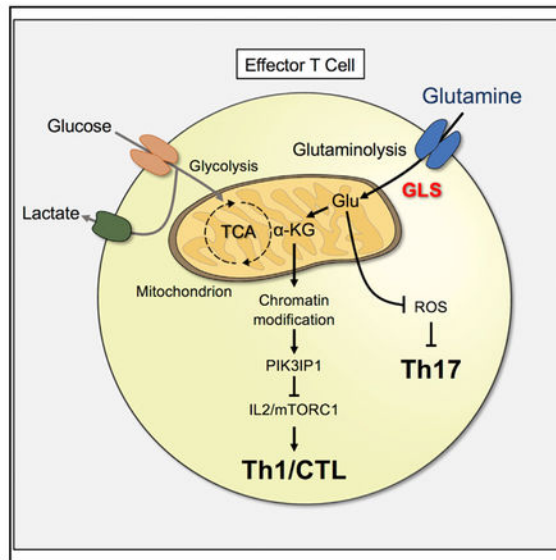
Supplemental Information includes seven figures and two tables and can be found with this article online at <https://doi.org/10.1016/j.cell.2018.10.001>.

DECLARATION OF INTERESTS

The authors declare no competing interests.

Activated T cells differentiate into functional subsets with distinct metabolic programs. Glutaminase (GLS) converts glutamine to glutamate to support the tricarboxylic acid cycle and redox and epigenetic reactions. Here, we identify a key role for GLS in T cell activation and specification. Though GLS deficiency diminished initial T cell activation and proliferation and impaired differentiation of Th17 cells, loss of GLS also increased Tbet to promote differentiation and effector function of CD4 Th1 and CD8 CTL cells. This was associated with altered chromatin accessibility and gene expression, including decreased PIK3IP1 in Th1 cells that sensitized to IL-2-mediated mTORC1 signaling. *In vivo*, GLS null T cells failed to drive Th17-inflammatory diseases, and Th1 cells had initially elevated function but exhausted over time. Transient GLS inhibition, however, led to increased Th1 and CTL T cell numbers. Glutamine metabolism thus has distinct roles to promote Th17 but constrain Th1 and CTL effector cell differentiation.

Graphical Abstract



In Brief

Glutamine metabolism, and its effects on chromatin, promotes Th17 but constrains Th1 and CTL effector cell differentiation.

INTRODUCTION

Stimulated T cells exit quiescence to proliferate and develop effector functions that are essential for immunity. To support the metabolic demands of an immune response, antigen receptor signals and co-stimulation activate the phosphatidylinositol-3 kinase (PI3K)/Akt/mTORC1 signaling pathway to induce Myc and metabolic flux through glycolysis and mitochondrial oxidative phosphorylation (Ho et al., 2015; Sena et al., 2013). Elevated glycolysis and mitochondrial production of reactive oxygen species also promote T cell calcium signaling (Ho et al., 2015; Sena et al., 2013) and specific effector functions, including transcription and translation of interferon- γ (IFN γ) (Chang et al., 2013; Jacobs et al., 2008; Peng et al., 2016) in activated Th1 CD4 T cells and CD8 T cells. Importantly, each

T cell subset utilizes and requires a distinct metabolic program (Michalek et al., 2011; Nakaya et al., 2014). If activated T cells fail to induce appropriate metabolic pathways, effector function and ability to induce inflammatory disease *In vivo* are impaired (Macintyre et al., 2014; Yin et al., 2015). How specific metabolic programs establish and promote the function of T cell subsets remains poorly understood but may allow selective modulation of immunity in inflammation and cancer.

In addition to increased use of glucose in activated effector T cells, glutamine uptake and glutaminolysis are also upregulated (Carr et al., 2010; Wang et al., 2011). Glutamine is a conditionally essential amino acid in rapidly proliferating cells (Curthoys and Watford, 1995) and a potential target in cancer treatment (DeBerardinis and Cheng, 2010; Cheng et al., 2011; Wise and Thompson, 2010). Activated T cells upregulate amino acid transporters (Sinclair et al., 2013) and enzymes that metabolize glutamine (Nakaya et al., 2014; Wang et al., 2011). Glutamine is initially hydrolyzed via the enzyme glutaminase (GLS) (Wang et al., 2010) to produce glutamate, which is used in protein synthesis and generation of glutathione to regulate reactive oxygen species (ROS) and exchanged to promote cystine uptake (Siska et al., 2016). Glutamate is further metabolized to α -ketoglutarate (α -KG), which provides anaplerotic support of the tricarboxylic acid cycle (TCA) cycle in growing cells (Yuan et al., 2014) and is a substrate for histone and DNA demethylases that regulate chromatin accessibility (Nakajima and Kunimoto, 2014).

In addition to effector T cell activation, glutamine metabolism is implicated in the establishment of specific CD4 T cell subsets. Glutamine deprivation or deletion of ASCT2 was shown to promote Foxp3 expression, the transcription factor of regulatory T cells (Treg) (Klysz et al., 2015; Nakaya et al., 2014). Inhibition or silencing of the glutamic-oxaloacetate transaminase 1 (GOT1) enzyme that mediates conversion of glutamate to α -KG led to a shift in differentiation of Th17 to Treg via methylation of the Foxp3 locus (Xu et al., 2017). Further, direct treatment of T cells with α -KG altered gene expression and chromatin methylation, in part through the CCCTC-binding factor (CTCF) (Chisolm et al., 2017).

Conversion of glutamine to glutamate by GLS may play a critical role in T cell function and fate. Although under investigation as a target to inhibit the metabolism of cancer cells (Cerione and Richard, 2010; DeBerardinis et al., 2008), the role of GLS in T cells has been unclear. Here, we explore whether inhibition of glutaminolysis at the level of GLS alters T cell effector function and show distinct T cell dependencies on this metabolic pathway.

RESULTS

GLS and Glutaminolysis Contribute to T Cell Metabolism upon Activation

Activated T cells have significant metabolic requirements to support proliferation and differentiation. To determine the relative roles of glucose and glutamine in these processes, intracellular metabolites were measured following activation of CD4 T cells. In addition to increased pyruvate and lactate, glutamate and α -KG levels increased, suggesting elevated glutamine metabolism (Figure 1A). Intracellular glutamate is primarily generated from glutamine by GLS or from α -KG and aspartate by GOT1 and GOT2 and is converted to α -KG by glutamate dehydrogenase 1 (GLUD1), which are each expressed in CD4 and CD8 T

cells (Figure S1A). The increased levels of both α -KG and glutamate, and high relative ratio of glutamine to glutamate (Figure S1B), suggested GLS as a key source of glutamate and α -KG. To determine the relative roles of glutaminolysis and glycolysis as fuels for mitochondrial metabolism, we measured oxygen consumption of stimulated T cells treated with mitochondrial pyruvate carrier (UK5099) or GLS (CB839) inhibitors. While neither UK5099 nor CB839 was sufficient to reduce T cell respiration alone, the combination led to a significant decrease in oxygen consumption (Figure 1B).

To directly determine how inhibition of GLS affects glucose metabolism, CD4 T cells were stimulated in uniformly labeled ^{13}C -glucose with or without CB839, and glucose-derived carbons were traced. As expected, inhibition of GLS led to increased intracellular glutamine and decreased glutamate (Figure 1C). Aspartate levels also decreased significantly. Glucose-derived ^{13}C was increased in both glutamate and aspartate, indicating a greater fraction of glucose contribution to synthesis of these amino acids. Serine and alanine overall abundance also decreased while glycine was unchanged, and each showed a decreased portion derived from glucose (Figure S1C). Overall levels of TCA intermediates were also reduced, yet with increased fractional labeling from glucose-derived ^{13}C (Figure 1D). Glycolytic intermediates were more abundant upon GLS inhibition, suggesting elevated glycolysis (Figure S1D). However, lactate levels and ^{13}C labeling were unchanged, and pyruvate levels decreased (Figure S1E). Anabolic pathways were also affected, and total levels of the nucleotide precursor N-carbamoyl-aspartate decreased (Figure S1F).

CD4 T Cell Subsets Have Distinct Programs of Glutamine Metabolism

Distinct cytokines led activated T cells to induce specific metabolic programs. Th1, Th17, and Treg cells (Gerriets et al., 2015) were examined to assess whether CD4 T cell subsets had different patterns and reliance on glutamine metabolism. T cells activated and differentiated into each subset showed increased glutamate and α -KG levels relative to naive T cells. This was most pronounced in Th17 cells (Figure 2A), which also had the highest relative ratio of glutamate to glutamine (Figure S2A). To test the role of glutamine and GLS in Th1, Th17, and Treg T cell subsets, CD4 T cells were differentiated with or without glutamine or with GLS inhibitor. Both Th1 and Th17 required glutamine, as glutamine-deficient media markedly reduced Th1 production of IFN γ and Th17 production of IL-17, yet GLS inhibition decreased cytokine production and proliferation only from Th17 cells and appeared to increase Th1 cytokine secretion (Figure 2B). Glutamine deficiency reduced proliferation at days 3 and 5 in both Th1 and Th17 cells. GLS inhibition impaired proliferation of both Th1 and Th17 cells after 3 days in culture (Figures 2C and 2D). Importantly, CB839-treated Th1 cells partially recovered proliferation by day 5. Glutamine deprivation also induced Treg under Th1 and Th17 skew conditions, yet GLS inhibition did not (Figure 2E).

Several enzymes contribute to regulation of glutaminolysis in T cells. Th17 cells had greater expression of GLS than Th1 at protein and RNA levels (Figures S2B and S2C). Th1 and Th17 cells expressed low levels of *Gls2* mRNA and expressed similar levels of other glutamine and anaplerotic metabolic enzymes (Figures S2C–S2E). Th1 and Th17 cells had distinct metabolic profiles, and intracellular metabolites shifted in both Th1 and Th17 cells

upon GLS inhibition, including alanine, aspartate, and glutamate metabolism pathways (Figure 2F; Table S1). Nutrient uptake and secretion also differed between Th1 and Th17 cells and were modified by GLS inhibition. Glutamine uptake and glutamate, pyruvate, and lactate secretion were higher in Th17 but reduced upon GLS inhibition (Figure S2F). GLS may contribute to cellular redox regulation through generation of glutamate for glutathione synthesis, and ROS increased in both Th1 and Th17 cells when treated with CB839 (Figure S2G).

GLS Deficiency Has Little Effect on Resting T Cells but Modulates Activation

A GLS^{fl/fl} model was generated and crossed to CD4-Cre to specifically delete GLS late in T cell thymic development to test the role of GLS in T cells. Although GLS^{fl/fl}CD4-Cre⁺ T cells efficiently deleted *Gls* compared to control GLS^{fl/fl} T cells (Figure 3A), lymphocyte frequencies and numbers were unaltered (Figure 3B). Treg cells have been previously shown to be increased by ASCT2 or GOT1 deficiency (Nakaya et al., 2014; Xu et al., 2017) but were unchanged with GLS deficiency. Resting GLS^{fl/fl}CD4-Cre⁺ CD4 T cells also had normal cell size and phenotype (Figure 3C).

GLS deficiency did, however, impact T cell activation. Measurement of lactate secretion showed that acute GLS inhibition did not impair immediate events in T cell activation to rapidly induce glycolysis (Figure S3A). However, *in vitro*-stimulated GLS-deficient T cells failed to efficiently undergo blastogenesis and increase in cell size in the first 2 days (Figure S3B). GLS-deficient CD4 T cells had reduced induction of CD25 and CD44 and downregulation of CD62L (Figure 3D) at 48 hr. In addition, *in vitro* accumulation of viable stimulated T cells was reduced by GLS deficiency (Figure S3C). By day 5 of stimulation in IL2 (Th0 conditions), however, GLS-deficient CD4 T cells had adapted, and activation markers were similar to control (Figure 3E).

Delayed activation-marker expression and proliferation of GLS-deficient T cells suggested impaired function and differentiation. Surprisingly, a greater frequency of GLS^{fl/fl}CD4-Cre⁺ T cells produced IFN γ after 5 days in Th0 conditions than did control T cells (Figures 3F and 3G). In addition, GLS-deficient cells that expressed IFN γ did so to a higher level than IFN γ -producing control T cells. IFN γ expression is regulated in part by the transcription factor, Tbet, and Tbet levels were elevated in activated GLS^{fl/fl}CD4-Cre⁺ Th0 T cells (Figure 3H). Similarly, inhibition of GLS with CB839 also led to greater expression of IFN γ and Tbet (Figures 3I–3K).

The ability of T cells to adapt to GLS deficiency and display enhanced function *in vitro* suggested that *In vivo* responses may be altered. Control and GLS^{fl/fl}CD4-Cre⁺ mice were immunized with 2W peptide to measure proliferation and IFN γ secretion. At 8 days after immunization, 2W peptide (EAWGALANWAVDSA)-major histocompatibility complex II (2W-MHC) tetramer binding CD4 T cells proliferated similarly regardless of GLS expression (Figures S3D and S3E). At day 15, IFN γ levels, however, were increased in GLS-deficient 2W-MHC tetramer binding T cells (Figure S3F). In contrast, proliferation to weaker homeostatic cues was reduced for GLS^{fl/fl}CD4-Cre⁺ T cells in both spleen and lymph node compared to wild-type T cells 5 days after transfer to recipient RAG1^{-/-} mice (Figure S3G).

Because cytotoxic CD8 T cells are also driven by Tbet (Knox et al., 2014), the dependence of CD8 T cells on GLS was assessed. Similar to CD4 cells, *in vitro*-stimulated GLS^{fl/fl}CD4-Cre⁺ CD8 T cells survived and accumulated less efficiently than control T cells (Figure S3H). Importantly, GLS^{fl/fl}CD4-Cre⁺ CD8 T cells had increased expression of the effector protein granzyme B (Figure 3L) and Tbet (Figure 3M). Acute inhibition of GLS with CB839 led to increased granzyme B and perforin after 5 days stimulation (Figures S3I and S3J). In addition to increased effector proteins, CB839-treated CD8 T cells expressed increased levels of Tbet and Eomes and markers of proliferation (Figures S3K–S3M). However, GLS inhibition also increased the portion of CD8 T cells that expressed the inhibitory receptors Lag3 and PD-1 (Figure S3O). GLS deficiency thus can impair initial activation and proliferation of CD4 and CD8 cells while promoting Th1-like and cytotoxic T lymphocyte (CTL) effector programs that may ultimately sensitize to inhibition.

GLS Plays Differential Roles in CD4 T Cell Effector Subsets

Given the differences in glutamine metabolism between Th1 and Th17 cells and spontaneous Th1-like differentiation with IL2 in Th0 conditions, we next tested whether GLS deficiency affected T cell subset specification and function. Control and GLS^{fl/fl}CD4-Cre⁺ CD4 T cells were differentiated *in vitro* into Th1 and Th17 subsets. Similar to Th0 cells, a greater percentage of GLS^{fl/fl}CD4-Cre⁺ T cells expressed IFN γ when in Th1-skewing conditions (Figures 4A and 4B). Conversely, a decreased percentage of GLS-deficient T cells expressed IL17A when in Th17-skewing conditions. Expression of effector molecules and differentiation in Th1, Th17, and Treg are regulated by Tbet, ROR γ t, and FoxP3, respectively, and GLS-deficient T cells showed increased Tbet under Th1 conditions and decreased ROR γ t under Th17 conditions (Figures 4C and 4D). FoxP3 expression was unchanged in the absence of GLS. Similar results to GLS knockout (KO) were obtained when GLS was acutely inhibited using CB839 in Th1-, Th17-, and Treg-skewing conditions (Figures S4A–S4D).

GLS deficiency promoted Th1 and suppressed Th17 differentiation and may affect plasticity and terminal fates. However, GLS-deficient T cells stimulated in Th17 conditions that failed to express ROR γ t and IL17 did not significantly elevate IFN γ or FoxP3 (Figures 2E, 4A, and S4A). In contrast, GLS-deficient T cells stimulated in Th1 conditions showed evidence of excessive effector function as the proportion of multifunctional Th1 cells (Figure 4E) as well as expression of KLRG1 and inhibitory receptors PD-1, Tim3, and Lag3 were elevated (Figures 4F, S4E, and S4F).

We next assessed how GLS inhibition affected Th1 and Th17 metabolism and differentiation over time. Steady-state levels of glutamine rapidly increased while glutamate and aspartate rapidly decreased in both Th1 and Th17 cells upon GLS inhibition (Figure 4G). While levels of these metabolites partially recovered in GLS inhibitor-treated Th1 cells starting on day 3, they remained low in treated Th17 cells. Likewise, oxidized glutathione (GSSG) recovered in Th1 but remained low in Th17. Similar trends of initial decrease followed by recovery in Th1 cells were observed in glycolytic and TCA cycle intermediates (Figures S4G and S4H). Consistent with impaired early metabolism, flux measurements showed that glucose uptake was reduced in both Th1 and Th17 cells on day 3 (Figure 4H). By day 5, however, Th1 cells

had increased levels of glucose uptake and glycolytic flux relative to controls, while Th17 remained impaired by GLS inhibition (Figures 4H and 4I).

Changes in metabolism occurred rapidly upon GLS inhibition and preceded Th1 and Th17 differentiation. Indeed, GLS inhibition led both Th1 and Th17 to have reduced levels of subset transcription factors and prevented an increase in cell size relative to control cells on days 1 and 2 after activation (Figures 4J and 4K). By day 5, however, Th1 cells had recovered and increased both cell size and Tbet expression. These data are consistent with overall changes in biomass, as total rRNA levels per cell were similar in GLS inhibitor- or control-treated T cells on day 3, but Th1 had increased and Th17 had decreased rRNA levels by day 5 of GLS inhibition (Figure S4I).

GLS Affects Gene Expression and Chromatin Accessibility

Deficient GLS activity may alter differentiation through production of cofactors, including α -KG and 2-hydroxyglutarate (2-HG), for epigenetic marks and changes in chromatin status (Reid et al., 2017; Xu et al., 2017). Intracellular levels of α -KG were reduced in CB839-treated Th1 but not Th17 cells, while 2-HG increased in both Th1 and Th17 (Figures S5A and S5B). Reduced α -KG in CB839-treated Th1 cells suggested that α -KG may become limiting to regulate Th1 differentiation and function. A cell-permeable α -KG analog, dimethyl 2-ketogluta-rate (DMaKG), was tested to determine whether provision of α -KG could restore normal Th1 specification of CB839-treated T cells (Figures 5A–5C). DMaKG did not reduce cytokine production in Th1 cells by itself. However, DMaKG rectified IFN γ production and Tbet expression of CB839-treated Th1 cells to control levels. In contrast, Th17 cells were not rescued by DMaKG, and IL17 production and ROR γ t were unchanged or further decreased (Figures 5A and 5D), suggesting a distinct mechanism of regulation for Th17 cells by GLS.

Changes in α -KG and 2-HG may alter histone methylation and chromatin accessibility that influence T cell differentiation (Xu et al., 2017). Histone trimethylation was globally assessed by flow cytometry. Initially, GLS inhibition led to increased H3K27 trimethylation (Figure 5E). At later time points when Th1 differentiation was enhanced, however, CB839-treated Th1 and Th17 cells were found to have decreased or increased global H3K27 trimethylation, respectively (Figure 5F). H3K4 trimethylation was similarly reduced or increased in Th1 and Th17 cells, respectively, at day 5 (Figure S5C). Consistent with altered regulation of demethylation as a cause of Th1 differentiation upon GLS inhibition, treatment of T cells with an inhibitor of the histone demethylase JMJD3 also led to increased cytokine production in Th1 but not Th17 cells at day 5 (Figure 5G).

The dependence of Th17 cells on GLS was not rescued by DMaKG, but Th17 cells can be highly sensitive to increased ROS (Gerriets et al., 2015). The glutathione mimic N-acetyl cysteine (NAC) was tested to rescue GLS-deficient Th17 cells. NAC treatment alone modestly reduced Th17 expression of IL17 and ROR γ t (Figure 5H) while decreasing IFN γ secretion by Th1 (Figure S5D). Th17 production of IL17 and expression of ROR γ t were partially restored to control levels when combined with CB839. The combination did not, however, increase Th1 production of IFN γ . Changes in Th17 inhibition by CB839 may be mediated through chromatin modifications as NAC also restored H3K27 trimethylation in

GLS-deficient Th17 cells to control levels (Figure 5I) yet had no effect on H3K27 trimethylation in Th1 cells (Figure S5E).

Because multiple epigenetic marks may be altered, we performed the assay for transposase-accessible chromatin sequencing (ATAC-seq) to determine whether GLS deficiency altered chromatin accessibility after 5 days of Th1 and Th17 differentiation. CB839-treated Th1 cells had more genes with regions of increased accessibility than genes with decreased accessibility (Figure 5J). Th17 cells, however, had more genes with regions of reduced accessibility. While partially overlapping, affected genes were largely distinct for Th1 and Th17 cells (Figure S5F). Key Th1 and Th17 genes showed changes, including the *Ifng* and *Ii17a/f* loci in Th1 and Th17 cells, respectively (Figure 5K). Further, Ingenuity Pathway analyses of genes with altered promoter accessibility in Th1 cells showed changes in networks of cell survival and inflammation (Figure S5G). Analysis of promoter regions with altered accessibility identified recognition motifs for canonical T cell differentiation transcription factors, including AP-1, ETS, and IRF (Figure S5H). These altered promoter regions were also enriched in CTCF recognition motifs, a DNA-binding protein recently implicated to mediate the effects of α -KG on chromatin state (Chisolm et al., 2017).

Because altered chromatin accessibility can influence gene expression and T cell differentiation, T cells were cultured in Th1 or Th17 conditions with vehicle or CB839 and examined by RNA sequencing. Of the 200 genes with the most significantly altered expression in CB839-treated Th1 cells, the majority showed increased expression (Figure 6A). Conversely, more of these genes were downregulated in Th17 cells. Functional annotation using gene set enrichment analyses showed that GLS inhibition led to upregulation of specific pathways including those related to cell cycle, mTORC1, Myc, and IL2 signaling (Table S2). Similar gene sets were downregulated in Th17 cells treated with CB839.

IL2 signaling activates mTORC1 to promote Myc signaling, glycolysis, and Th1 effector differentiation (Boyman and Sprent, 2012; Chisolm et al., 2017). Given enrichment in these pathways by RNA sequencing (RNA-seq), the contribution of IL2/mTORC1 signaling was tested to increase effector function of GLS-deficient Th1 cells. Levels of the mTORC1 downstream target phospho-S6 were measured in Th1 and Th17 cells differentiated in IL2 and the presence or absence of CB839. GLS inhibition led to increased phospho-S6 in Th1 and decreased phospho-S6 in Th17 cells (Figure 6B). IL2 played a key role to promote phospho-S6, as increased phospho-S6, IFN γ , and Tbet in CB839-treated Th1 were dependent on IL2 (Figures 6C and S6A). Consistent with mTOR regulation of Myc protein, GLS inhibition modestly increased Myc in Th1 but not Th17 cells (Figure S6B). Importantly, while GLS inhibition in the presence of IL2 led to enhanced differentiation and a hypomethylated state, T cells hypermethylated H3K27 upon treatment with CB839 in the absence of IL2 (Figure S6C). The role of mTORC1 signaling in GLS-mediated regulation of Th1 cells was directly tested by treatment of cells on day 3 after activation with rapamycin. While rapamycin treatment at this time had no effect on control Th1 cells, it reduced phospho-S6 and cytokine production in CB839-treated Th1 cells (Figures 6D and S6D). A similar mechanism may occur for regulation of Th0 and CTL, as GLS inhibition also led to enhanced phospho-S6 for these cells in the presence of IL2 (Figure S6E).

Several regulators of mTORC1 signaling were altered by GLS inhibition in Th1 cells by RNA-seq, including *Pik3ip1*, *Akt*, *Tsc2*, *Sestrin2*, and *Castor1* (Figure S6F). Of these, *Pik3ip1*, which has been shown to suppress PI3K and mTORC1 in T cells (DeFrances et al., 2012; Wei et al., 2016), was most strongly downregulated in Th1 cells by GLS inhibition. Restoring PIK3IP1 in CB839-treated Th1 cells by retroviral transduction was sufficient to reduce phospho-S6 and cytokine secretion (Figures 6E and S6G). Conversely, CRISPR genetic deletion of *Pik3ip1* in primary T cells led to increased phospho-S6 and IFN γ production (Figures 6F and S6H). PIK3IP1 is a transmembrane protein, and treatment of stimulated T cells with anti-PIK3IP1 antibody directed against the extracellular domain suppressed phospho-S6 (Figure 6G) and T cell activation as evidenced by down-regulation of CD25, CD44, and CD62L (Figures 6H and S6I). Together, these data suggest that PIK3IP1 levels can contribute to mTORC1 activity and effector function in Th1 cells, while Th17 cells are dependent on GLS-mediated regulation of cellular redox state.

GLS Regulates *In vivo* for Inflammatory Effector T Cell Responses

We next tested whether Th17 cells require GLS to elicit inflammation *In vivo*. Allogeneic bone marrow was transplanted alone or with control and GLS^{fl/fl}CD4-Cre⁺ T cells to induce a model of IL17-dependent chronic graft-versus-host disease (cGvHD). Recipient mice were weighed regularly, and GLS-deficient allogeneic T cells led to less weight loss than control T cells (Figure S7A). cGvHD is a multi-organ disease (Panoskaltsis-Mortari et al., 2007), and mouse models of cGvHD include lung inflammation. Histological examination showed that GLS-deficient T cells reduced lung immune infiltrate and clinical inflammation score (Figures 7A and 7B) and caused significantly less airway functional impairment than control T cells (Figure S7B). Immunologically, GLS deficiency reduced IL17-producing CD4 cells, with a trend toward reduced IFN γ (Figure 7C). GLS was also critical in an independent model of Th17-mediated lung inflammation, in which control and GLS-deficient animals were sensitized and challenged in the airway with house dust mite antigen, and lipopolysaccharide (LPS) failed to accumulate CD4 T cells and produce inflammatory cytokine in the lung (Figure S7C). Inflammatory bowel disease (IBD) also involves Th17 cells, and we found that while adoptive transfer of control T cells led to weight loss and inflammation, mice that received GLS-deficient T cells maintained weight (Figure 7D). Despite partial protection from disease, a greater percentage of GLS-deficient T cells in the mesenteric lymph nodes produced IFN γ , consistent with a preferential Th1 response (Figure S7D).

The role of GLS deficiency to enhance Th1 and CTL function was next tested *In vivo*. Control and GLS^{fl/fl}CD4-Cre⁺ T cells were evaluated in a murine chimeric antigen receptor (CAR) model for the ability to eliminate endogenous target B cells and persist *In vivo*. T cells were *in vitro* transduced with CAR T expression vectors either lacking a cytoplasmic tail () or with a CD3 ζ -CD28 (28- ζ) intracellular tail and adoptively transferred into animals conditioned with cyclophosphamide. 14 days after T cell transfer, endogenous CD19-expressing B cells were significantly reduced by both control and GLS^{fl/fl}CD4-Cre⁺ CAR T cells (Figure 7E). After 28 days, however, B cells had accumulated in recipients of GLS^{fl/fl}CD4-Cre⁺ CAR T cells and were fully recovered in lymph nodes by day 42 (Figures

7E and 7F). Consistent with upregulation of inhibitory receptors upon activation, GLS-deficient T cells appeared unable to sustain an effector response *In vivo*.

Because GLS inhibition altered chromatin accessibility in Th1 cells *in vitro*, it was possible that transient treatment with CB839 could induce long-lasting effect. T cells were treated with vehicle or CB839 during *in vitro* transduction to express CARs and tested for subsequent *In vivo* function. Vehicle- and CB839-treated CAR T cells were equally capable of eliminating CD19⁺ targets *In vivo* (Figure S7E). Importantly, *in vitro* CB839-treated 28- ζ CAR T cells accumulated *In vivo* to a greater extent than untreated CAR T cells (Figure 7G) and showed greater ability to eliminate B cell leukemia cells *in vitro* (Figure 7H). This increased ability of Th1 and CD8 effector T cells to proliferate or persist following transient GLS inhibition was not specific to CAR T cells. CD8 T cells bearing a Pmel-specific T cell receptor (TCR) transgene treated with CB839 *in vitro* prior to adoptive transfer also accumulated to greater numbers *In vivo* by day 7 when challenged with an antigen-expressing vaccinia virus (Figure 7I), and increased cell numbers persisted for greater than 5 weeks (Figure 7J). Thus, chronic or complete GLS deficiency impairs T cell responses *In vivo*, while transient *in vitro* inhibition may enhance subsequent Th1 and CD8 CTL effector function and long-lasting cell numbers *In vivo*.

DISCUSSION

T cell activation and specification into functional subsets requires increased biosynthesis and establishment of the appropriate gene expression program. Importantly, the metabolic requirements of each subset are distinct, and Th1, Th17, and Treg have critical metabolic differences that influence their differentiation and fate. While glucose metabolism has been extensively studied, here we show that glutamine metabolism and GLS activity regulate T cell activation to promote Th17 while impairing Th1 differentiation and effector function.

Glutamine and generation of α -KG through GLS and glutaminolysis can play a key role to maintain levels of TCA intermediates. Indeed, acute GLS inhibition lowered T cell respiration and abundance of TCA intermediates while increasing glucose contribution to these pathways. In effector T cell populations, however, this association becomes context dependent as IL2 can promote a GLS-independent Th1-like phenotype in CD4 T cells and enhance CD8 CTL effector function. Th17 cells, however, remain GLS dependent. For Th1 and cytotoxic CD8 T cells to adapt to GLS deficiency, an alternate anaplerotic source is essential and pyruvate carboxylase may generate oxaloacetate from glycolysis-derived pyruvate, as can occur in glutamine-independent cancers (Cheng et al., 2011).

While GLS acts on glutamine to facilitate the first event of glutaminolysis, modulation of glutamine metabolism at different steps can lead to strikingly different phenotypes. The absence of glutamine prevented cytokine production and proliferation of both Th1 and Th17 cells and instead promoted Treg generation. Deficiency of the glutamine transporter ASCT2 suppressed proliferation, impaired both Th1 and Th17 T cell specification, and enhanced Treg generation (Nakaya et al., 2014). Suppression of GOT1, which converts aspartate and α -KG to glutamate and oxaloacetate, impaired Th17 with increased Treg differentiation (Xu et al., 2017). GLS deficiency differs to selectively promote Th1 and impair Th17

differentiation while not affecting Treg. Subset-specific protein expression and levels of different metabolites in glutamine-related pathways may mediate these distinct responses. ASCT2 is one of multiple glutamine transporters and may interact with the CARMA1 complex upon T cell activation to regulate NF- κ B signaling (Nakaya et al., 2014). GOT1 deficiency may restrict glutamate production from aspartate while leaving glutamine conversion to glutamate and α -KG intact. GLS deficiency, in contrast, allows glutamine uptake but leads to both glutamate and aspartate deficiencies and increased ROS. Glutamate and glutamine can be generated from other sources, such as aspartate, which can be p53 dependent and induce cell survival in glutamine-limiting conditions (Tajan et al., 2018). Given the interconnections of each metabolite in these pathways, it is likely that inhibition of this metabolic network leads to context-specific outcomes.

Glutamine-dependent metabolites may influence T cells through alteration of epigenetic marks and chromatin accessibility. Increased cytosolic acetyl-CoA levels can modulate histone acetylation and can regulate IFN γ expression (Peng et al., 2016), and α -KG can play an important role in histone and DNA methylation. Individual histone marks have distinct regulatory roles, and while we found consistent changes in global H3K4 and H3K27 trimethylation that differentially influenced gene expression, other marks likely also affect chromatin status as a whole to determine gene expression. Changes in the abundance of α -KG, TCA cycle intermediates, and 2-HG likely contribute to altered chromatin state and gene expression. The initial hyper-methylation phenotype continued in Th17 but reversed Th1 cells by IL2, suggesting that IL2-induced signals and Th1 differentiation ultimately dominate the overall chromatin accessibility and gene expression patterns. While inhibition of JMJD3 demethylase by GSKJ4 phenocopies CB839 treatment in Th1 cells, other epigenetic modifiers also likely contribute to this differential response. ROS also promoted increased histone methylation in GLS-inhibited Th17 cells and influenced cytokine production by Th1 cells, although the mechanisms are unclear. One protein that may play a central role in GLS regulation of chromatin is CTCF, which was shown to regulate IL-2-dependent gene programming in T cells in response to α -KG (Chisolm et al., 2017). While *Ctcf* mRNA levels were not strongly affected in this study by either Th1 or Th17 GLS-deficient T cells, CTCF consensus-binding sequences were significantly enriched in chromatin sites identified as altered in ATAC-seq studies. The shared occurrence of CTCF-binding sites may represent an initial α -KG-dependent response and lead to more open or closed chromatin based on other DNA-binding factors and transcription factor expression differences in Th1 and Th17 cells.

Opposing effects of GLS inhibition on mTORC1 signaling in Th1 and Th17 and the ability of mTORC1 to promote a glycolytic and effector differentiation program suggest that this pathway plays a key role to mediate the effects of GLS on T cell fate. IL2 was essential to stimulate mTORC1 activity that enhanced differentiation of GLS-deficient Th1 cells. GLS inhibition induced several changes in IL2 and mTORC1 signaling that may contribute to the differential response of Th1 and Th17. In addition to increased Sestrin2 and Castor1 that are involved in amino acid sensing (Chantranupong et al., 2014; Wolfson and Sabatini, 2017) and Akt1, PIK3IP1 was sharply downregulated in GLS-deficient Th1 cells. This transmembrane protein was expressed at a low level in Th17 cells and is inhibitory to the mTOR signaling pathway by binding PI3K p110 and inhibiting PI3K activity. It has been

shown to suppress liver carcinomas (He et al., 2008) and inhibit T cell activation (DeFrances et al., 2012; Wei et al., 2016). Manipulation of PIK3IP1 expression and deletion here demonstrates that this protein may also contribute to GLS inhibition to modulate mTORC1 signaling in Th1 cells. Conversely, Th17 cells can respond poorly to IL2 (Quintana et al., 2012), and reduced IL2 response or altered PI3K/Akt/mTORC1 activating signal may also impair differentiation in GLS-deficient Th17 cells.

Targeting GLS may selectively impair Th17 cells while having the potential to enhance Th1 responses *In vivo*. Th17 cells were GLS dependent and failed to induce lung inflammation in either cGvHD or acute airway inflammation models, and GLS deficiency protected against inflammatory bowel disease. In addition, inhibition of GLS was recently shown to suppress a model of rheumatoid arthritis (Takahashi et al., 2017), although mechanisms were uncertain. Th1 cells were also impaired in these models, potentially due to the lower levels of inflammation or the eventual impairment of Th1 cells due to induction of inhibitory receptors. Similarly, GLS-deficient CAR T cells were initially competent to eliminate B cell targets *In vivo* but failed over time. Transient *in vitro* GLS inhibition, however, enhanced effector activity and allowed CAR T cells and antiviral T cells to accumulate to greater numbers *In vivo*. This effect is likely due to GLS-inhibition-induced changes to chromatin accessibility and sensitization to cytokine signals that promote sustained function in a setting where T cells are capable of performing glutaminolysis.

Subset-specific integration of glucose and glutamine metabolism may now offer new opportunities to modulate immunity. We propose that reduced α KG upon GLS inhibition leads to an initial increase in histone methylation that contributes to decreased PIK3IP1 expression and sensitization to IL2 signals in Th0, Th1, and CTL. Increased IL2 activation of mTORC1 signaling then promotes metabolic adaptation and results in a cumulative shift in epigenetic marks and chromatin status consistent with effector differentiation. In contrast, increased ROS caused by GLS inhibition promotes closed chromatin to prevent Th17 cell differentiation, which cannot be rescued by IL2, although molecular mechanisms remain uncertain. Glutaminolysis thus both promotes Th17 and suppresses Th1 responses, and GLS may provide a target to treat inflammation *In vivo* with continuous inhibition. Conversely, transient inhibition may program T cells for enhanced IFN γ -specific effector responses. GLS is a promising candidate to inhibit cancer cell metabolism, and it may be important to consider transient or episodic GLS inhibition to epigenetically reprogram T cells for enhanced effector function and immunotherapy.

STAR★METHODS

CONTACT FOR REAGENT AND RESOURCE SHARING

Further information and requests for resources and reagents should be directed to and will be fulfilled by the Lead Contact, Dr. Jeffrey Rathmell (Jeff.rathmell@vumc.org).

EXPERIMENTAL MODEL AND SUBJECT DETAILS

Animals—With exception of GLS^{fl/fl} mice, which were generated as described below, all mice were obtained from the Jackson laboratory or described previously. All mouse

procedures were performed under Institutional Animal Care and Utilization Committee (IACUC)-approved protocols from Duke University, Vanderbilt University (2W tetramer, IBD, homeostatic proliferation, and asthma models), the National Cancer Institute (Vaccinia model), the Moffitt Cancer Center and Research Institute (CAR T cell *In vivo* model), and the University of Minnesota (Graft versus Host Disease model) and conformed to all relevant regulatory standards. Mice were housed in specific pathogen-free facilities in ventilated cages with at most 5 animals per cage and provided *ad libitum* food and water. With the exception of homeostatic proliferation studies, which used RAG1^{-/-} immunodeficient C57BL/6J mice, all studies used immunocompetent C57BL/6J mice that were treatment-naïve until the start of study.

GLS1^{fl/fl} animals were generated from GlS^{tm1a(KOMP)Mbp} embryonic stem cells (Project ID: CSD29307) from the KOMP that were blastocyst microinjected to generate mice (Duke University Transgenic and Knockout Shared Resource) and crossed to FLP transgenic animals. Progeny were then crossed with CD4-CRE transgenic mice to develop the GLS1^{fl/fl} CD4-CRE (GLS KO). In all cases comparing wild-type to GLS KO, healthy, sex-matched and age-matched littermates were used (male and female, 8 to 14 weeks of age unless otherwise stated). No sex differences in phenotype were noted in WT and GLS KO CD4 T cells. Animals were genotyped for floxed alleles and CRE allele.

Male C57BL/6J mice aged 8–16 weeks were used for *in vitro* CB839 experiments (RRID: IMSR_JAX:000664).

Cell Lines and *In Vitro* cultures—T cell *in vitro* experiments were carried out using primary mouse T cell cultures from male and female mice at 37°C with 5% CO₂ in RPMI media (CAT#10–40-CV) supplemented with HEPES, β-mercaptoethanol, Pen/Strep, and glutamine, unless otherwise stated. Generation of viral particles was performed in PLAT-E retroviral packing cell lines (Cell Biolabs). T cell killing assays were performed on CD19 expressing Emu cell lines (Generous gift from Dr. Davila Lab).

METHOD DETAILS

T cell *in vitro* activation and skew experiments—CB839 was dosed at 1 μM (activation) or 500 nM (differentiation), GSKJ4 (Cat#:S7070) at 1 μM, dimethyl-2-oxoglutarate (DMaKG) (Cat#: 349631) at 1.5 mM. and/or rapamycin (Cat#: 553210) at 5 nM. Briefly, CD4⁺ T cells were isolated (Cat#130-104-454) from wild-type animals (WT) and GLS1^{fl/fl} CD4-CRE⁺ mice (GLS KO) and activated over various time points via 5 ug/mL anti-CD3/anti-CD28 antibodies plate bound (CD3: Cat # 16-0031-85, CD28: Cat # 16-0281-85). Non-stimulated CD4 samples were maintained using 10 ng/mL IL-7 (Cat#: 217–17). For skewing experiments, naïve CD4 T cells from WT or KO animals were plated with αCD3 (as above) and subset-specific cytokines and antibodies (Th1: IL-12p70, αIFNγ, αIL4; Th17: IL6, αIFNγ, TGFβ, Treg: TGFβ and stimulated with feeder layer of irradiated splenocytes. Th0 experiments were run in skewing condition (+αCD3 antibody) without additional cytokines. After 3 days, cells were split with fresh media and stimulated with or without 10 ng/mL IL-2 (Cat#:14-8021-64) for a further 2 days. For intracellular cytokine stains, cells were re-stimulated using PMA/ionomycin in the presence of GolgiPlug (Cat#:

555029) for 4 hours, then fixed and stained for intracellular subset-specific cytokines using fix/perm kit (Cat#: 554714). For all other intracellular or intranuclear stains such as transcription factor, pS6, C-MYC, H3K4me3, H3K27me3, and total H3 protein, cells were removed from media, stained for surface markers (See Key Resources antibodies table), fixed, then stained for intracellular proteins using fix/perm kit (Cat# 00-5223-56, 00-5123-43). Cell proliferation was assessed by staining naive CD4⁺ cells with Cell Trace Violet proliferative dye at 5 μ M (Cat#: c34557).

Homeostatic Proliferation—Homeostatic proliferation was measured as previously described (Jacobs et al., 2010). Briefly, naive CD4⁺ and CD8⁺ T cells were isolated from male GLS^{fl/fl}CD4-Cre and wild-type Thy1.1⁺ mice. Cells were mixed in a 1:1 ratio and stained with proliferative dye Cell-Trace Violet (Cat#: c34557). Cells were transplanted by i.v. injection into recipient RAG knockout mice (RRID:IMSR_JAX:002216) 8 weeks of age. Five days after injection, spleen and mesenteric lymph node were collected, homogenized, and stained with antibodies against CD4, CD8, and Thy1.1 for flow cytometry analysis.

ATAC-Sequencing Experiments—Crude nuclei pellets for ATAC-seq were isolated according to Buenrostro et. al (Buenrostro et al., 2013) with modifications. Briefly, naive CD4 T cells from C57BL/6J mice were skewed to Th1 and Th17 subsets *in vitro* with vehicle or in the presence of 0.5 μ M CB839. At Day 5, T cells were re-isolated for CD4⁺ cells using CD4⁺ negative selection kit (Cat#: 130-104-454). 1×10^5 cells were removed for nuclei extraction in ATAC-Seq lysing buffer. Cells were exposed to Tn5+adaptor proteins from Nextera prep kit (Cat#: FC-121–1030) for 30 min at 37°C and immediately placed on ice. Transposed eluate was amplified via PCR using NEBNext High-fidelity 2x PCR mix (Cat#:M0541) and multiplexed (Cat#: FC-121–1011). Samples were purified using Zymo DNA cleanup kit (Cat#: D4011). QC of samples was run on bioanalyzer before being sent for sequencing.

RNA Sequencing Experiments—Naive CD4⁺ T cells from C57BL/6J mice were skewed to Th1 and Th17 subsets with or without CB839 over 5 days and total RNA extracted for RNaseq (Cat#: 74104). RNA was sent to VANDerbilt Technologies for Advanced GENomics (VANTAGE) core at Vanderbilt University. Libraries were prepared using 50ng of total RNA using the NEBNext Ultra RNA Library Kit for Illumina (Cat# E7530) and sequenced on HiSeq3000 at 75bp paired-end. Each sample was analyzed in triplicate. Sequencing reads were aligned against the Mouse GENCODE genome, Version M14 (January 2017 freeze, GRCm38, Ensembl 89) using the Spliced Transcripts Alignment to a Reference (STAR) software (Mudge and Harrow, 2015). Reads were preprocessed and index using SAMtools (Li et al., 2009). Mapped reads were assigned to gene features and quantified using featureCounts (Liao et al., 2014). Normalization and differential expression was performed using DESeq2 (Love et al., 2014). Skewed lymphocytes with and without CB839 were compared in both Th1 and Th17 groups. The top most significantly differentially expressed genes (FDR < 0.01 and Log2 difference greater than 0.5 in magnitude) were considered for subsequent functional enrichment using Geneset Enrichment Analysis. The top 200 most differentially expressed genes were used for unsupervised hierarchical cluster analysis and visualized using heatmap representations.

PCR—Pan T cells from WT or GLS KO mice were isolated and purified using Miltenyi isolation kit (Cat#: 130-095-130). Genomic DNA was generated using Kapa express Extract kit (Cat#: KR0370). Primers targeted over exon 10 and exon 11 were generated for wild-type band with a melting temperature of 54°C:

Forward: ACGAGAAAGTGGAGATCG

Reverse: GCCTTCTGGAAAACA

PCR product was then run on a 1% agarose gel with ethidium bromide and visualized by GelDoc XR (Cat#: 1708195).

Glucose Uptake—Glucose uptake assays were performed as previously described (Macintyre et al., 2014). Naive CD4⁺ T cells from C57BL/6J mice were differentiated into Th1 and Th17 cells, in triplicate, in the presence or absence of CB839 over five days and spun down after reisolation using CD4 kit as previously described. At day 3 and 5, cells were removed, washed twice in PBS, counted, then rested in 1 mL Kreb's Ringers HEPES (KRH) for at least 10 minutes. Cells were spun and resuspended to 5×10⁵ cells/50 μL KRH for glucose uptake assay. Briefly, ³H-2-deoxyglucose (Cat#: NET549001MC) was suspended in KRH bubble layered in oil (50:50 Dinonyl phthalate:Silicon 550, Cat#: 80151, Cat#: 784198), and cells were added to this bubble. Cells were incubated for 10 minutes at 37°C. Immediately after incubation, reaction was quenched with 200 μM phloretin (Cat#: 524488). Cells were spun, washed, and then resuspended in scintillation fluid for counting on Beckman-Coulter scintillation counter (3H, 1 min/sample read).

Extracellular Flux Analyses (Seahorse)—Experiments were carried out on Agilent Seahorse XF96 bioanalyzer (Agilent). Briefly, wild-type CD4⁺ cells from C57BL/6J mice were isolated as previous and activated for 3 days on αCD3/CD28 coated plates as previously described, or skewed to Th1 and Th17 subsets as described above. T cells were isolated and spun onto XF96 Cell-Tak (BD Bioscience, Cat#: 354240) coated plates and rested in Seahorse XF RPMI 1640 media supplemented with glutamine, sodium pyruvate, and glucose. For immediate metabolic response, 1 μM CB839 and 5 μM UK5099 (Cat#: PZ0160–5MG) were injected separately or in combination, and OCR and ECAR measured. For activation response, 1 μM CB839 was injected into IL-7 maintained naive CD4⁺ T cells in seahorse medium and allowed to incubate for 20 minutes, followed by soluble αCD3/CD28 injection. Mito Stress assay was performed using kit (Cat#103015–100).

Mass Spectrometry

¹³C Tracing: To measure ¹³C-Glucose tracing in T cell activation, CD4⁺ cells from C57BL/6J mice were stimulated on 5 μg/mL anti-CD3/CD28 for 3 days. At day 3, cells were pooled, washed 3x in PBS, and re-stimulated in presence of 1 μM CB839 or Vehicle (DMSO) and 11 mM ¹³C glucose (Cambridge Isotope Labs, Cat#CLM-1396–1). Cells were incubated for 24 hours at 37°C, then scraped and combined in triplicate. Cells were rinsed with 0.9% saline and metabolites were extracted in methanol. Metabolites measured by LC-High-Resolution Mass Spectrometer (LC-HRMS) using a Q-Exactive machine as previously described (Liberti et al., 2017). The time-dependent glucose labeling pattern was modeled as with the following equation:

$$\frac{[X^*]}{X^T} = 1 - e^{-\frac{f_X}{X^T}t}$$

In which $[X^*]$ is the concentration of labeled glucose, X^T is the total concentration (both labeled and unlabeled) of glucose, f_X is the glucose production flux. This model was fit to glucose MIDs using the fit() function in MATLAB to determine relative glucose production fluxes. Relative glucose pool sizes were estimated from MS signal intensities.

Differentiation: CD4⁺ cells were isolated as previously described and differentiated in subset-specific medium in the presence of vehicle or CB839 (in triplicate) for 3 days, split at day 3 with new media and IL-2, then allowed to incubate a further 2 days. At day 5, wells were combined, cells washed 1x in MACS buffer and re-isolated for CD4 via AutoMACS Pro automated magnetic separator (Miltenyi, Cat#: 130-092-545). Metabolites from Th1 and Th17 cells were extracted and analyzed by LC-High-Resolution Mass Spectrometer (LC-HRMS) using a Q-Exactive as described previously (Gerriets et al., 2015). Data were range scaled and analyzed using Metaboanalyst 3.5 (Xia and Wishart, 2002) (<http://www.metaboanalyst.ca/faces/home.xhtml>) to generate heatmaps and for principle component analyses.

Immunoblotting—Immunoblots were performed as previously described (Jacobs et al., 2008) with the following modifications. Cells lysed with RIPA buffer and Halt protease/phosphatase cocktail inhibitors (Life Tech, Cat#: 78443). Protein was quantified by Pierce BCA kit II (Cat#: 23227). Actin blots were visualized by near infrared fluorescence via Li-Cor Odyssey imager. GLS blots were visualized by chemiluminescence using anti-rabbit conjugated horseradish peroxidase. The antibodies used for westerns were: GLS (Cat#: GTX81012, 1:1000), β -Actin (Cat#: 8226, 1:10,000).

Viral Infection with PIK3IP1—Naive CD4⁺ T cells were isolated from wild-type C57BL/6J mice. T cells were stimulated in Th1 and Th17 skewing conditions plus vehicle of CB839 as previously described. These were incubated for 16 hours with a feeder layer of irradiated splenocytes. Plasmid constructs MSCV-PIK3IP-IRES-Thy1.1 (“PIK3IP1”) and control vector MSCV-IRES-Thy1.1 (“Control”) were used to transfect Plat-E cells (Cat#RV-101). T cells were then infected with cell supernatant containing retrovirus and polybrene and rested for 48 hours. Cells were split at Day 3 in new media containing 10 ng/mL IL-2 (Cat#14-8021-64) and then incubated for 48 hours before removing for intracellular cytokine and transcription factor staining by flow cytometry as described above.

CRISPR/CAS9 PIK3IP1—Naive CD4⁺ T cells were isolated from Cas9 transgenic mice (RRID:IMSR_JAX:024858) aged 10–12 weeks old. T cells were plated on an α CD3/CD28 coated 24-well plate and one day after activation, cells were transduced with viral supernatant prepared from PLAT-E cells (Cat#RV-101) transfected with a solution of 2000 μ g DNA (empty vector pMx-U6-empty-GFP or two different PIK3IP1 targeting guide RNA containing vectors pMx-U6-PIK3IP1-GFP). T cells with the viral particles were centrifuged

at 2000rpm for 2 hours at 37°C, followed by incubation for 2 hours at 37°C and 5% CO₂. The media was then replaced with 1mL fresh Th1 skewing media and incubated overnight. This was repeated a second time on day 2 of T cell activation. Cells were collected ten days post activation for pS6, intracellular cytokine production, and transcription factor staining by flow cytometry as described.

PIK3IP1 Antibody *in vitro*—Naive CD4⁺ T cells were isolated from C57BL6 mice and activated on aCD3/CD28-coated 24 well plates at 1×10⁶ cells/well with either control antibody (Cat#bs-0295P) or PIK3IP1 antibody (Cat#16826-1-AP) at 0.5 µg/mL. Cells were incubated at 37°C for 72 hours and cells removed at 24, 48, and 72 hours for flow cytometry analysis of activation.

***In vivo* Graft Versus Host Disease**—Induction of Graft versus Host Disease (cGVHD) was performed as previously described (Panoskaltis-Mortari et al., 2007). Briefly, female mice aged 13–14 weeks were lethally irradiated the day before bone marrow transplant. Mice were dosed with cyclophosphamide (Cytosan, Bristol Myers Squibb) at 120 mg/kg/day on days –3 and –2. Recipient irradiated mice were transplanted via caudal vein with 15 × 10⁶ T cell depleted allogeneic marrow with 1 × 10⁶ cells splenic CD4⁺ cells from WT or GLS KO mice, or control (no CD4⁺ T cells). Mice were assessed for lung elasticity, resistance, and compliance at Day 28 by whole body plethysmography using the Flexivent system (Scireq, Montreal, PQ, Canada). Histological assessment of GVHD was assessed as previously described (Blazar et al., 1998).

Asthma Model—Female WT or GLS KO mice at 24 weeks of age were administered intranasal sensitization of either PBS alone or a combination of 100 µg house dust mite extract (Cat#XPB70D3A2.5) and 0.1 µg LPS from *Escherichia coli* 0111:B4 (Cat#L4391) in 50 µL of PBS. Sensitizations were performed on Day 0, 7, and 14. Mice were harvested 24 hours post-challenge, and lung homogenates were digested to single cells and analyzed for cytokine production and transcription factors by flow cytometry.

***In vivo* Vaccinia Viral Response**—Spleens from pmel-1 Ly5.1 (B6.Cg-Thy-1a/Cy Tg [TcrαTcrβ] 8Rest/J) mice were used to generate a single cell suspension and treated with ACK buffer to lyse red blood cells. Splenocytes were stimulated *in vitro* with 1 µM human glycoprotein 100 nine-mer peptide (hgp100_{25–33}) and expanded in culture medium containing IL-2 for 7 days along with 1 µM CB839 or DMSO vehicle. Subsequently, one million CD8⁺ cells from each condition were transferred by IV injection into recipient 6 week old female Ly5.2 C57BL/6 mice. Immediately following transfer, mice were infected with rhgp100 vaccinia virus (1 × 10⁷ plaque-forming units (PFU)). At the indicated time points following transfer, recipient mouse blood or tissues were collected for analysis.

Immunization with 2W peptide—10–14 week old male GLS WT and KO animals were injected with 10 µg 2W peptide (Genscript) emulsified with Complete Freund's Adjuvant (Cat#F5881) or PBS control and injected subcutaneously in the rear flank as previously described (Moon et al., 2007) and rested for 8 days. At day 8, inguinal lymph nodes and spleens were removed and isolated. MHCII-specific CD4 cells were isolated and purified with APC-conjugated tetramers (generously provided by Dr. Marc Jenkins laboratory,

Minneapolis, MN) using Miltenyi LS magnetic columns (Cat#130-042-401) and stained for extracellular and intracellular targets. Intracellular IFN γ was measured in a separate experiment on day 15 after immunization.

***In vitro* CAR T cell co-culture with target E μ B ALL cells**—T cells were isolated from wild-type C57BL6 spleens using the Pan T Cell isolation kit (Cat#: 130-095-130) and were activated on anti-CD3 anti-CD28 coated plates with IL2 for four days with or without CB839. On days 1 and 2, T cells were transduced with retrovirus produced by Plat-E cells carrying the CAR 28- ζ construct targeting CD19 with GFP reporter. On day 4, CAR T cells were washed three times to remove any drug remnants and plated to equal concentrations on a 96 well plate at 5×10^5 cells per well and serial dilutions thereof. 5×10^5 Emu cells, a CD19+ B cell acute lymphoblastic leukemia cell line (Generously provided by Dr. Davila Lab) were then added to every well to assay cell numbers. CD19+ and GFP+ events were stained and counted by flow for each well after 72 hours.

***In vivo* CAR T cells**—CAR T cells were produced as previously described (Li et al., 2017). Briefly, spleen T cells were isolated from wild-type B6, Thy1.1, or GLS KO mice at day 0. Cells were then activated with mouse CD3/CD28 Dynabeads and 30 IU/mL recombinant human IL2. At day 1 and 2, cells were spin transduced twice with retrovirus carrying CARs. At day 3, cells were fed with fresh medium. At day 4, transduced T cells were harvested, beads removed, evaluated for viability, transduction efficiency, immune phenotype and ready for use. For CB839 treated CAR T cells, compound was added to the culture at day 1, 2 and 3. For *In vivo* study, C57B6 mice (n = 25) were i.p. injected with cyclophosphamide (Cat#C0768) at 300 mg/kg. Mice were i.v. injected with 3×10^5 CAR T cells one day after CTX injection. Peripheral blood (PB) samples were collected after CAR T injection, stained with B cell and T cell antibodies and subjected to flow cytometry. CountBright beads were added to measure B and T cell numbers.

Colitis/IBD Induction—Colitis was induced by adoptive transfer of 0.4×10^6 purified (> 99% purity) CD4⁺CD25⁻CD45RB^{hi} cells i.p. into recipient male RAG KO mice (RRID: IMSR_JAX:002216). Spleen and lymph node suspensions were used first to purify CD4⁺ cells using magnetic bead cell separation with a StemCell Kit and these cells were stained with anti-CD4, anti-CD25 and anti-CD45RB for further flow sorting using a FACS Diva flow cytometer (Becton Dickinson) with purities over 95% of the indicated populations. Mice that received adoptive transfers of different cell genotypes were always cohoused in the same cages to avoid differences due to microbiota composition divergence during colitis development. Mice were treated with the NSAID Piroxicam to induce gut damage and initiate disease and animals were weighed over time. Mice that reached humane endpoints and were euthanized were maintained in the analysis at the final weight. At the end of the experiment, mesenteric lymph nodes were isolated and single cell suspensions were analyzed for cytokine production.

QUANTIFICATION AND STATISTICAL ANALYSIS

Statistical analyses were performed with Prism software version 7.01 (GraphPad Software, La Jolla California, USA, <https://www.graphpad.com>) using the Student's t test, one-way

ANOVA, or one-sample t test. Longitudinal data was analyzed by two-way ANOVA followed by Tukey's test and followed up with one-way ANOVA or t test at one specific time point as specified. Statistically significant results are indicated (* $p < 0.05$, ** $p < 0.01$, *** $p < 0.001$) and ns indicates select non-significant data. Error bars show mean \pm Standard Deviation unless otherwise indicated. All experiments were carried out in triplicate technical and biological replicates unless otherwise stated. FACs plots shown are representative of $n = 3$ replicates. RNA-Seq data were analyzed by DESeq2 (Love et al., 2014) in R (Team, 2017).

DATA AND SOFTWARE AVAILABILITY

RNASeq data have been deposited in the GEO database under accession number GEO: GSE112244. ATACSeq data have been deposited in the ArrayExpress database under accession number ArrayExpress: E-MTAB-6648.

Supplementary Material

Refer to Web version on PubMed Central for supplementary material.

ACKNOWLEDGMENTS

We thank members of the Rathmell lab and H. Hu (University of Alabama, Birmingham) for providing MSCV-PIK3IP-IRES-Thy1.1 and control retroviral constructs, T. Dileepan and M.K. Jenkins (University of Minnesota) for providing reagents for 2W immunization and tetramer staining, and J. Cools (VIB) for providing pMx-U6 plasmids. Some CB839 for *in vitro* studies was generously provided by Calithera Biosciences. This research was funded by the National Institutes of Health R01 HL136664 (J.C.R.), R01 DK105550 (J.C.R.), R01 CA217987 (J.C.R., W.K.R.), R01CA193256 (J.W.L.), and P30CA01423 (J.W.L.).

REFERENCES

- Blazar BR, Taylor PA, McElmurry R, Tian L, Panoskaltis-Mortari A, Lam S, Lees C, Waldschmidt T, and Vallera DA (1998). Engraftment of severe combined immune deficient mice receiving allogeneic bone marrow via In utero or postnatal transfer. *Blood* 92, 3949–3959. [PubMed: 9808589]
- Boyman O, and Sprent J (2012). The role of interleukin-2 during homeostasis and activation of the immune system. *Nat. Rev. Immunol* 12, 180–190. [PubMed: 22343569]
- Buenrostro JD, Giresi PG, Zaba LC, Chang HY, and Greenleaf WJ (2013). Transposition of native chromatin for fast and sensitive epigenomic profiling of open chromatin, DNA-binding proteins and nucleosome position. *Nat. Methods* 10, 1213–1218. [PubMed: 24097267]
- Carr EL, Kelman A, Wu GS, Gopaul R, Senkevitch E, Aghvanyan A, Turay AM, and Frauwirth KA (2010). Glutamine uptake and metabolism are coordinately regulated by ERK/MAPK during T lymphocyte activation. *J. Immunol* 185, 1037–1044. [PubMed: 20554958]
- Cerione JWE, and Richard A (2010). Glutaminase: A Hot Spot For Regulation Of Cancer Cell Metabolism? *Oncotarget* 1, 734–740. [PubMed: 21234284]
- Chang CH, Curtis JD, Maggi LB, Jr., Faubert B, Villarino AV, O'Sullivan D, Huang SC, van der Windt GJ, Blagih J, Qiu J, et al. (2013). Post-transcriptional control of T cell effector function by aerobic glycolysis. *Cell* 153, 1239–1251. [PubMed: 23746840]
- Chantranupong L, Wolfson RL, Orozco JM, Saxton RA, Scaria SM, Bar-Peled L, Spooner E, Isasa M, Gygi SP, and Sabatini DM (2014). The Sestrins interact with GATOR2 to negatively regulate the amino-acid-sensing pathway upstream of mTORC1. *Cell Rep.* 9, 1–8. [PubMed: 25263562]
- DeBerardinis RJ, and Cheng T (2010). Q's next: the diverse functions of glutamine in metabolism, cell biology and cancer. *Oncogene* 29, 313–324. [PubMed: 19881548]

- Cheng T, Sudderth J, Yang C, Mullen AR, Jin ES, Matés JM, and DeBerardinis RJ (2011). Pyruvate carboxylase is required for glutamine-independent growth of tumor cells. *Proc. Natl. Acad. Sci. USA* 108, 8674–8679. [PubMed: 21555572]
- Chisolm DA, Savic D, Moore AJ, Ballesteros-Tato A, Leon B, Cross-man DK, Murre C, Myers RM, and Weinmann AS (2017). CCCTC-Binding Factor Translates Interleukin 2- and alpha-Ketoglutarate-Sensitive Metabolic Changes in T Cells into Context-Dependent Gene Programs. *Immunity* 47, 251–267.e7. [PubMed: 28813658]
- Curthoys NP, and Watford M (1995). Regulation of glutaminase activity and glutamine metabolism. *Annu. Rev. Nutr* 15, 133–159. [PubMed: 8527215]
- Davila ML, Kloss CC, Gunset G, and Sadelain M (2013). CD19 CAR-targeted T cells induce long-term remission and B Cell Aplasia in an immuno-competent mouse model of B cell acute lymphoblastic leukemia. *PLoS ONE* 8, e61338. [PubMed: 23585892]
- DeBerardinis RJ, Lum JJ, Hatzivassiliou G, and Thompson CB (2008). The biology of cancer: metabolic reprogramming fuels cell growth and proliferation. *Cell Metab.* 7, 11–20. [PubMed: 18177721]
- DeFrances MC, Debelius DR, Cheng J, and Kane LP (2012). Inhibition of T-cell activation by PIK3IP1. *Eur. J. Immunol* 42, 2754–2759. [PubMed: 22706993]
- Gattinoni L, Zhong X-S, Palmer DC, Ji Y, Hinrichs CS, Yu Z, Wrzesinski C, Boni A, Cassard L, Garvin LM, et al. (2009). Wnt signaling arrests effector T cell differentiation and generates CD8+ memory stem cells. *Nat. Med* 15, 808–813. [PubMed: 19525962]
- Gerriets VA, Kishton RJ, Nichols AG, Macintyre AN, Inoue M, Ilkayeva O, Winter PS, Liu X, Priyadharshini B, Slawinska ME, et al. (2015). Metabolic programming and PDHK1 control CD4+ T cell subsets and inflammation. *J. Clin. Invest* 125, 194–207. [PubMed: 25437876]
- He X, Zhu Z, Johnson C, Stoops J, Eaker AE, Bowen W, and DeFrances MC (2008). PIK3IP1, a negative regulator of PI3K, suppresses the development of hepatocellular carcinoma. *Cancer Res.* 68, 5591–5598. [PubMed: 18632611]
- Ho P-C, Bihuniak JD, Macintyre AN, Staron M, Liu X, Amezquita R, Tsui YC, Cui G, Micevic G, Perales JC, et al. (2015). Phosphoenolpyruvate Is a Metabolic Checkpoint of Anti-tumor T Cell Responses. *Cell* 162, 1217–1228. [PubMed: 26321681]
- Jacobs SR, Herman CE, MacIver NJ, Wofford JA, Wieman HL, Hammen JJ, and Rathmell JC (2008). Glucose Uptake Is Limiting in T Cell Activation and Requires CD28-Mediated Akt-Dependent and Independent Pathways. *J Immunol* 180, 4476–4486. [PubMed: 18354169]
- Jacobs SR, Michalek RD, and Rathmell JC (2010). IL-7 Is Essential for Homeostatic Control of T Cell Metabolism *In vivo*. *J Immunol* 184, 3461–3469. [PubMed: 20194717]
- Klysz D, Tai X, Robert PA, Craveiro M, Cretenet G, Oburoglu L, Mongellaz C, Floess S, Fritz V, Matias MI, et al. (2015). Glutamine-dependent α -ketoglutarate production regulates the balance between T helper 1 cell and regulatory T cell generation. *Sci. Signal* 8, ra97. [PubMed: 26420908]
- Knox JJ, Cosma GL, Betts MR, and McLane LM (2014). Characterization of T-bet and eomes in peripheral human immune cells. *Front. Immunol* 5, 217. [PubMed: 24860576]
- Li G, Park K, and Davila ML (2017). Gammaretroviral Production and T Cell Transduction to Genetically Retarget Primary T Cells Against Cancer In T-Cell Differentiation: Methods and Protocols, Lugli E, ed. (New York, NY: Springer New York), pp. 111–118.
- Li H, Handsaker B, Wysoker A, Fennell T, Ruan J, Homer N, Marth G, Abecasis G, and Durbin R; 1000 Genome Project Data Processing Subgroup (2009). The Sequence Alignment/Map format and SAMtools. *Bioinformatics* 25, 2078–2079. [PubMed: 19505943]
- Liao Y, Smyth GK, and Shi W (2014). featureCounts: an efficient general purpose program for assigning sequence reads to genomic features. *Bioinformatics* 30, 923–930. [PubMed: 24227677]
- Liberti MV, Dai Z, Wardell SE, Baccile JA, Liu X, Gao X, Baldi R, Mehrmohamadi M, Johnson MO, Madhukar NS, et al. (2017). A Predictive Model for Selective Targeting of the Warburg Effect through GAPDH Inhibition with a Natural Product. *Cell Metab.* 26, 648–659.e8. [PubMed: 28918937]
- Love MI, Huber W, and Anders S (2014). Moderated estimation of fold change and dispersion for RNA-seq data with DESeq2. *Genome Biol.* 15, 550. [PubMed: 25516281]

- Macintyre AN, Gerriets VA, Nichols AG, Michalek RD, Rudolph MC, Deoliveira D, Anderson SM, Abel ED, Chen BJ, Hale LP, and Rathmell JC (2014). The glucose transporter Glut1 is selectively essential for CD4 T cell activation and effector function. *Cell Metab.* 20, 61–72. [PubMed: 24930970]
- Michalek RD, Gerriets VA, Jacobs SR, Macintyre AN, MacIver NJ, Mason EF, Sullivan SA, Nichols AG, and Rathmell JC (2011). Cutting edge: distinct glycolytic and lipid oxidative metabolic programs are essential for effector and regulatory CD4⁺ T cell subsets. *J. Immunol* 186, 3299–3303. [PubMed: 21317389]
- Moon JJ, Chu HH, Pepper M, McSorley SJ, Jameson SC, Kedl RM, and Jenkins MK (2007). Naive CD4(+) T cell frequency varies for different epitopes and predicts repertoire diversity and response magnitude. *Immunity* 27, 203–213. [PubMed: 17707129]
- Mudge JM, and Harrow J (2015). Creating reference gene annotation for the mouse C57BL/6J genome assembly. *Mamm. Genome* 26, 366–378. [PubMed: 26187010]
- Nakajima H, and Kunimoto H (2014). TET2 as an epigenetic master regulator for normal and malignant hematopoiesis. *Cancer Sci.* 105, 1093–1099. [PubMed: 25040794]
- Nakaya M, Xiao Y, Zhou X, Chang JH, Chang M, Cheng X, Blonska M, Lin X, and Sun SC (2014). Inflammatory T cell responses rely on amino acid transporter ASCT2 facilitation of glutamine uptake and mTORC1 kinase activation. *Immunity* 40, 692–705. [PubMed: 24792914]
- Overwijk WW, Tsung A, Irvine KR, Parkhurst MR, Goletz TJ, Tsung K, Carroll MW, Liu C, Moss B, Rosenberg SA, and Restifo NP (1998). gp100/pmel 17 is a murine tumor rejection antigen: induction of “self”-reactive, tumoricidal T cells using high-affinity, altered peptide ligand. *J. Exp. Med* 188, 277–286. [PubMed: 9670040]
- Panoskaltzis-Mortari A, Tram KV, Price AP, Wendt CH, and Blazar BR (2007). A new murine model for bronchiolitis obliterans post-bone marrow transplant. *Am. J. Respir. Crit. Care Med* 176, 713–723. [PubMed: 17575098]
- Peng M, Yin N, Chhangawala S, Xu K, Leslie CS, and Li MO (2016). Aerobic glycolysis promotes T helper 1 cell differentiation through an epigenetic mechanism. *Science* 354, 481–484. [PubMed: 27708054]
- Quintana FJ, Jin H, Burns EJ, Nadeau M, Yeste A, Kumar D, Rangachari M, Zhu C, Xiao S, Seavitt J, et al. (2012). Aiolos promotes TH17 differentiation by directly silencing Il2 expression. *Nat. Immunol* 13, 770–777. [PubMed: 22751139]
- Reid MA, Dai Z, and Locasale JW (2017). The impact of cellular metabolism on chromatin dynamics and epigenetics. *Nat. Cell Biol* 19, 1298–1306. [PubMed: 29058720]
- Sena LA, Li S, Jairaman A, Prakriya M, Ezponda T, Hildeman DA, Wang CR, Schumacker PT, Licht JD, Perlman H, et al. (2013). Mitochondria are required for antigen-specific T cell activation through reactive oxygen species signaling. *Immunity* 38, 225–236. [PubMed: 23415911]
- Sinclair LV, Rolf J, Emslie E, Shi YB, Taylor PM, and Cantrell DA (2013). Control of amino-acid transport by antigen receptors coordinates the metabolic reprogramming essential for T cell differentiation. *Nat. Immunol* 14, 500–508. [PubMed: 23525088]
- Siska PJ, Kim B, Ji X, Hoeksema MD, Massion PP, Beckermann KE, Wu J, Chi J-T, Hong J, and Rathmell JC (2016). Fluorescence-based measurement of cystine uptake through xCT shows requirement for ROS detoxification in activated lymphocytes. *J. Immunol. Methods* 438, 51–58. [PubMed: 27594594]
- Sukumar M, Liu J, Ji Y, Subramanian M, Crompton JG, Yu Z, Roychoudhuri R, Palmer DC, Muranski P, Karoly ED, et al. (2013). Inhibiting glycolytic metabolism enhances CD8⁺ T cell memory and antitumor function. *J. Clin. Invest* 123, 4479–4488. [PubMed: 24091329]
- Tajan M, Hock AK, Blagih J, Robertson NA, Labuschagne CF, Kruiswijk F, Humpton TJ, Adams PD, and Vousden KH (2018). A Role for p53 in the Adaptation to Glutamine Starvation through the Expression of SLC1A3. *Cell Metab* 10.1016/j.cmet.2018.07.005.
- Takahashi S, Saegusa J, Sendo S, Okano T, Akashi K, Irino Y, and Morinobu A (2017). Glutaminase 1 plays a key role in the cell growth of fibroblast-like synoviocytes in rheumatoid arthritis. *Arthritis Res. Ther* 19, 76. [PubMed: 28399896]
- Team RC (2017). R: A language and environment for statistical computing (Vienna, Austria: R Foundation for Statistical Computing).

- Toffalini F, Kallin A, Vandenberghe P, Pierre P, Michaux L, Cools J, and Demoulin J-B (2009). The fusion proteins TEL-PDGFRbeta and FIP1L1-PDGFRalpha escape ubiquitination and degradation. *Haematologica* 94, 1085–1093. [PubMed: 19644140]
- Wang JB, Erickson JW, Fuji R, Ramachandran S, Gao P, Dinavahi R, Wilson KF, Ambrosio AL, Dias SM, Dang CV, and Cerione RA (2010). Targeting mitochondrial glutaminase activity inhibits oncogenic transformation. *Cancer Cell* 18, 207–219. [PubMed: 20832749]
- Wang R, Dillon CP, Shi LZ, Milasta S, Carter R, Finkelstein D, McCormick LL, Fitzgerald P, Chi H, Munger J, and Green DR (2011). The transcription factor Myc controls metabolic reprogramming upon T lymphocyte activation. *Immunity* 35, 871–882. [PubMed: 22195744]
- Wei H, Geng J, Shi B, Liu Z, Wang YH, Stevens AC, Sprout SL, Yao M, Wang H, and Hu H (2016). Cutting Edge: Foxp1 Controls Naive CD8+ T Cell Quiescence by Simultaneously Repressing Key Pathways in Cellular Metabolism and Cell Cycle Progression. *J. Immunol* 196, 3537–3541. [PubMed: 27001958]
- Wise DR, and Thompson CB (2010). Glutamine addiction: a new therapeutic target in cancer. *Trends Biochem. Sci* 35, 427–433. [PubMed: 20570523]
- Wolfson RL, and Sabatini DM (2017). The Dawn of the Age of Amino Acid Sensors for the mTORC1 Pathway. *Cell Metab.* 26, 301–309. [PubMed: 28768171]
- Wu Y, Borde M, Heissmeyer V, Feuerer M, Lapan AD, Stroud JC, Bates DL, Guo L, Han A, Ziegler SF, et al. (2006). FOXP3 controls regulatory T cell function through cooperation with NFAT. *Cell* 126, 375–387. [PubMed: 16873067]
- Xia J, and Wishart DS (2002). Using MetaboAnalyst 3.0 for Comprehensive Metabolomics Data Analysis. *Curr Protoc Bioinformatics*. 10.1002/cpbi.11.
- Xu T, Stewart KM, Wang X, Liu K, Xie M, Ryu JK, Li K, Ma T, Wang H, Ni L, et al. (2017). Metabolic control of T_H17 and induced T_{reg} cell balance by an epigenetic mechanism. *Nature* 548, 228–233. [PubMed: 28783731]
- Yin Y, Choi S-C, Xu Z, Perry DJ, Seay H, Croker BP, Sobel ES, Brusko TM, and Morel L (2015). Normalization of CD4+ T cell metabolism reverses lupus. *Sci Transl Med* 7, 274ra218.
- Yuan Q, Song Y, Yang CH, Jan LY, and Jan YN (2014). Female contact modulates male aggression via a sexually dimorphic GABAergic circuit in *Drosophila*. *Nat. Neurosci* 17, 81–88. [PubMed: 24241395]

Highlights

- T cells utilize GLS to support glutaminolysis that integrates with glycolysis
- GLS promotes differentiation and function of Th17 cells yet restrains Th1 cells
- GLS alters chromatin and gene expression to enhance IL2 and mTORC1 signaling
- Targeting GLS protects from Th17 and enhances Th1 cells but can lead to exhaustion

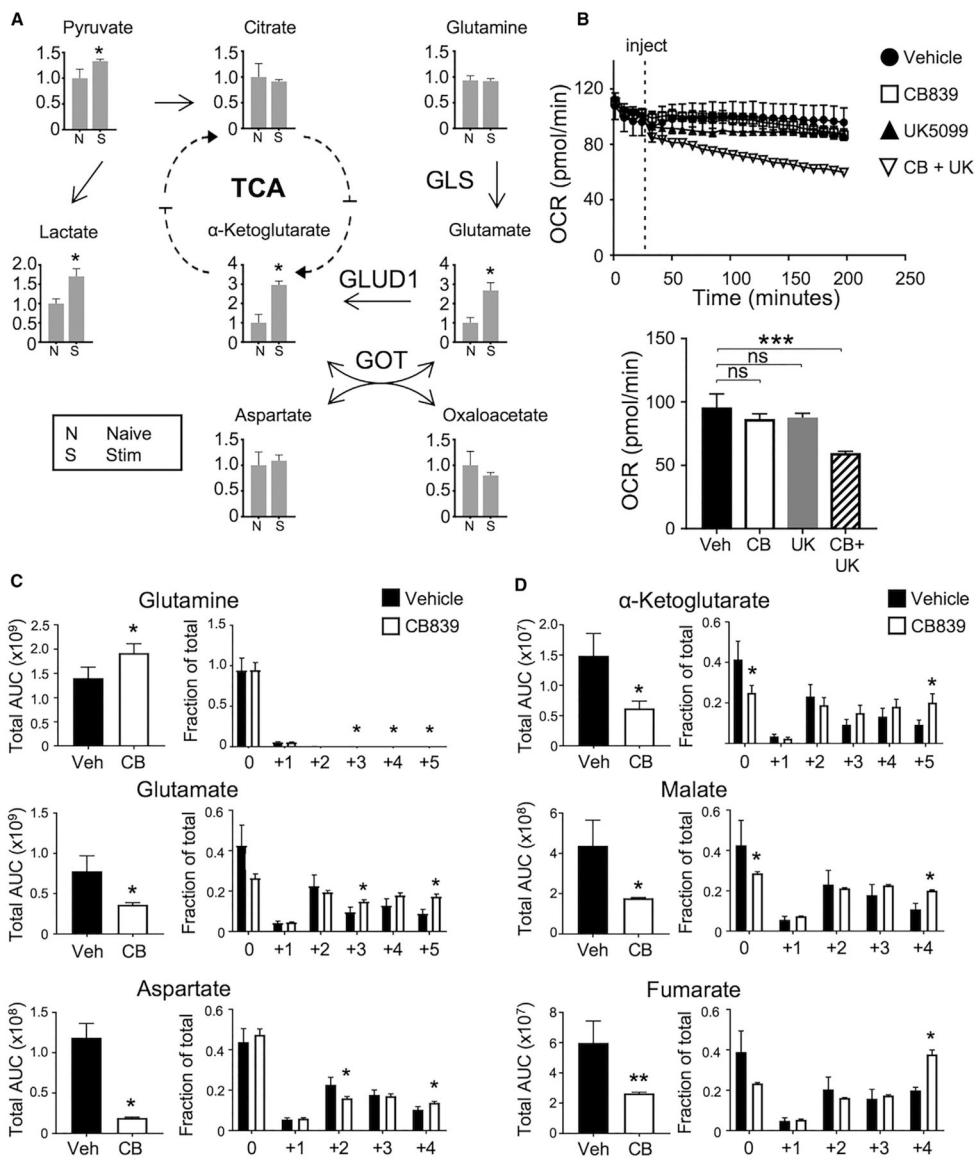


Figure 1. Activated T Cells Rely on Both Glucose and Glutamine to Sustain Cell Metabolism
 (A) Metabolites extracted for mass spectrometry and presented as fold change from naive in T cells stimulated for 16 hr (S) or naive (N) conditions (one-way ANOVA).
 (B) Oxygen consumption rate (OCR) assayed from naive CD4 cells from wild-type (WT) mice stimulated for 3 days on α CD3/CD28, injected with drug described (top). OCR at time point 200 min (bottom, one-way ANOVA).
 (C and D) Abundance of metabolites (left, unpaired t test) and fractional labeling (right, one-way ANOVA) of stimulated CD4⁺ T cells in the presence of CB839 and ¹³C-glucose for glutaminolytic intermediates (C) and TCA intermediates (D).
 Also see Figure S1.

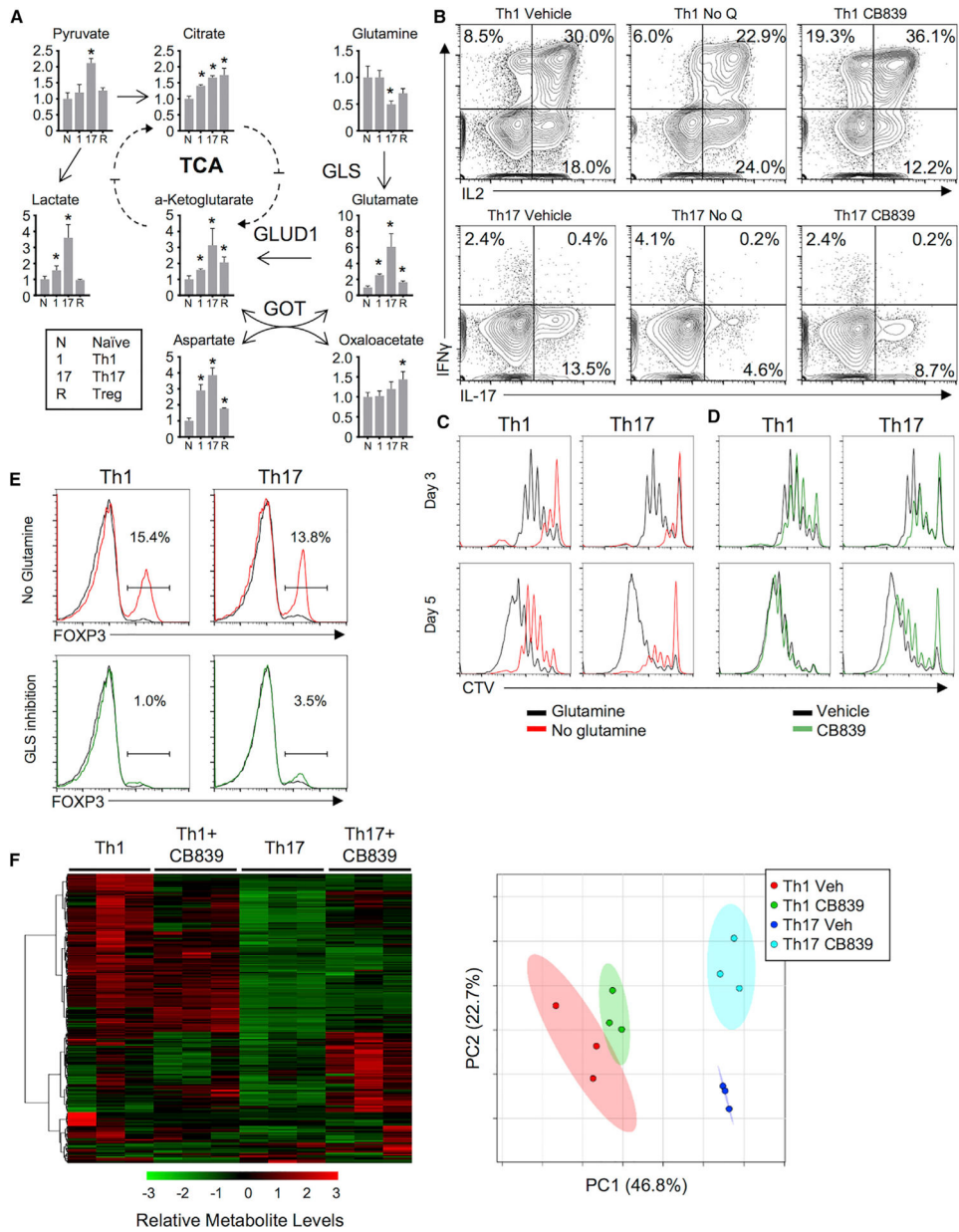


Figure 2. Th1 and Th17 Cells Differ in Their Use of Glutaminolysis, and GLS Deficiency Is Distinct from Glutamine Deficiency

(A) Metabolite fold change from naive in wild-type CD4⁺ cells maintained in IL-7 (N) or differentiated for 5 days into Th1 (1), Th17 (17), or Treg (R) cells (one-way ANOVA).
 (B) Cytokine production from Th1 (top) and Th17 (bottom) differentiated T cells in the presence of glutamine (left), absence of glutamine (middle), or presence of GLS1-inhibitor CB839 (right).
 (C) Proliferation of cell trace violet (CTV)-labeled T cells stimulated and differentiated in Th1 or Th17 conditions with (black lines) or without (red lines) glutamine after 3 and 5 days of culture.
 (D) Same as in (C), but with vehicle (black lines) or CB839 (green lines).

(E) Foxp3 expression in CD4 T cells activated in Th1- or Th17-skewing conditions in glutamine deficient (red, left) conditions or in the presence of CB839 (green, right).
(F) Heatmap (left) and principle component analysis (right) of metabolites from Th1 and Th17 cells with or without CB839.
Also see Figure S2 and Table S1.

Author Manuscript

Author Manuscript

Author Manuscript

Author Manuscript

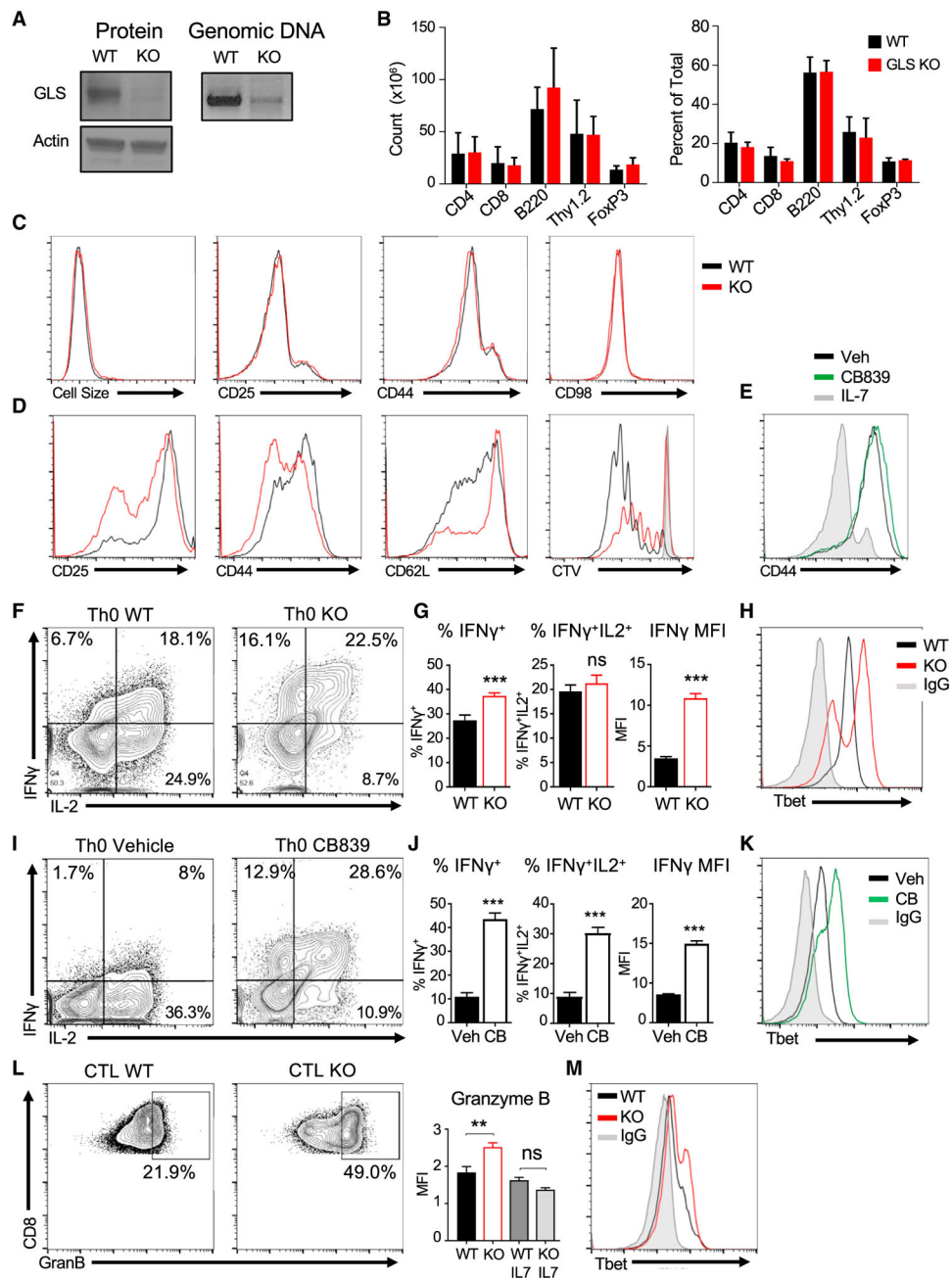


Figure 3. GLS Is Dispensable for T Cell Homeostasis but Constrains Development of a Th1-like Phenotype

(A) Immunoblot (left) and genomic DNA (right) in isolated Pan T cells (CD4⁺ and CD8⁺) from GLS^{f1/f1} CD4-Cre⁺ (GLS KO) and littermate wild-type controls (WT).

(B) Cell counts (left) and percent of total splenocytes (right) from WT and GLS KO animals. No significance versus wild-type, one-way ANOVA.

(C and D) Flow cytometry analysis of T cell activation markers and cell size of CD4⁺ T cells (C) freshly isolated from WT and GLS KO T spleens or (D) activation markers and proliferation of WT and GLS KO CD4⁺ T cells activated on α CD3/CD28 over 48 hr.

(E) Flow cytometry analysis of CD44 in CB839- or vehicle-treated T cells activated on α CD3/CD28 at day 5.

(F–K) Naive CD4⁺ T cells activated without cytokines over 3 days, split with IL-2, then stimulated to measure cytokines on day 5. (F) Cytokine production of wild-type and GLS KO T cells. (G) Average percent total IFN γ ⁺ producers (left), percent double positive IFN γ ⁺IL2⁺ producers (middle), and the median fluorescence intensity (MFI) (right) of all IFN γ ⁺ cells in (F) (unpaired t test). (H) Tbet protein expression in WT, GLS KO, and isotype control T cells. Representative of n = 2 experiments. (I–K) Same as in (F–H), except with GLS-inhibitor CB839 and vehicle.

(L and M) CD8⁺ T cells from WT or GLS KO animals activated on α CD3/CD28 + IL2 for 5 days. (L) Expression of CD8⁺ granzyme B protein at day 5 (left) and average of granzyme B MFI signal (right) (Student's t test, n = 3 replicates/group). (M) Tbet protein expression in WT, GLS KO, and isotype control (representative of n = 2 experiments).

Also see Figure S3.

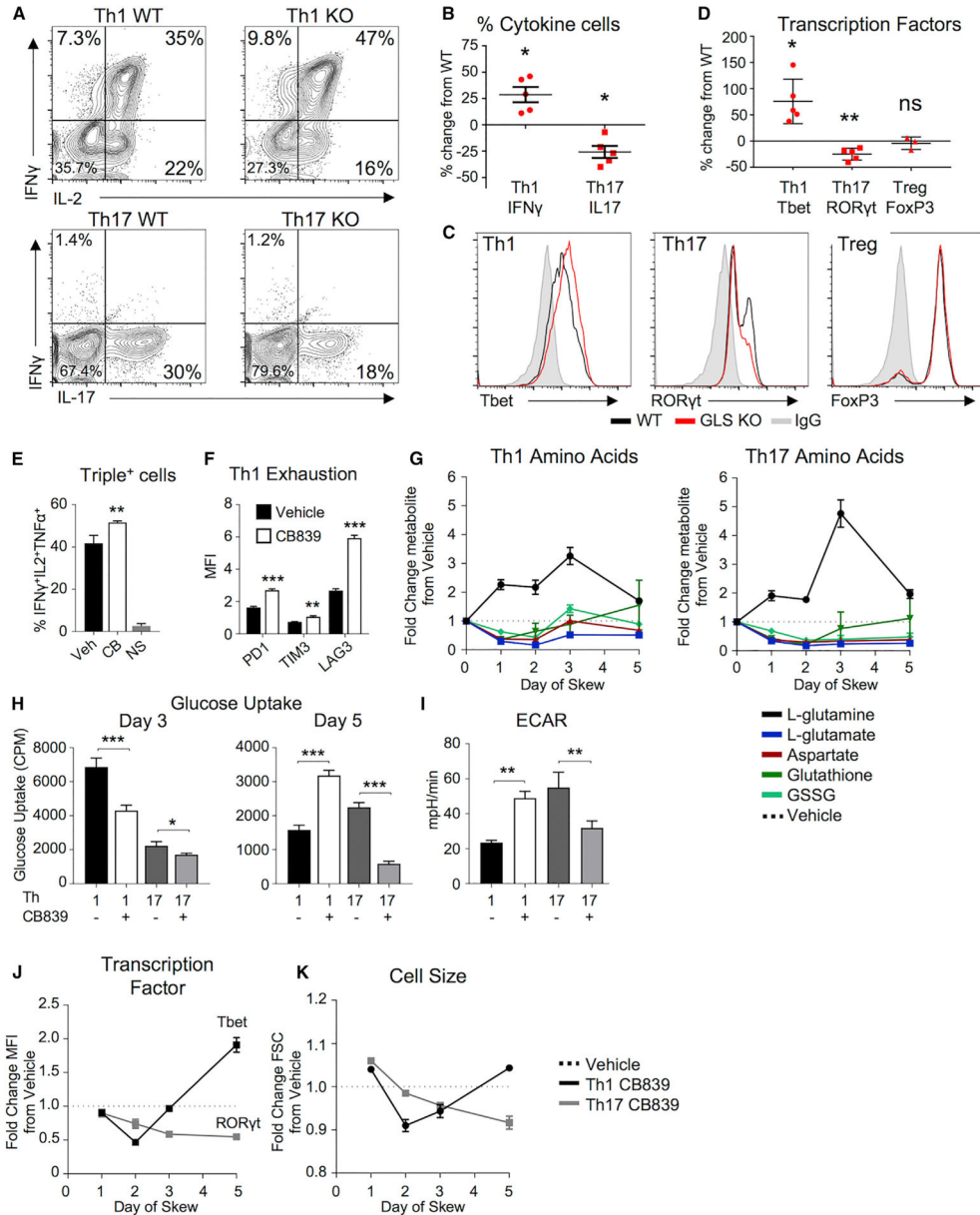


Figure 4. GLS Specifies Th1 and Th17 Differentiation and Metabolism

(A–D) Naive CD4⁺ T cells from WT and GLS KO T cells differentiated in Th1-, Th17-, or Treg-skewing media over 5 days. (A) IFN γ and IL2 production in Th1-skewing conditions (top) and IL-17 production in Th17-skewing conditions (bottom). (B) Average percent change cytokine producers in Th1 and Th17 cells from WT (paired t test). (C) Transcription factor expression of Th1, Th17, and Treg cells in WT (black) and GLS KO (red). (D) Average percent change from WT of transcription factors (one-sample t test) in GLS KO T cells.

(E–K) WT CD4⁺ T cells differentiated in Th1 or Th17 conditions in the presence of vehicle or CB839 over 5 days. (E) Percent of Th1 cells producing IFN γ , IL2, and TNF α at day 5 (unpaired Student’s t test; NS, no stim). (F) Median fluorescence intensity of inhibitory

receptors (two-way ANOVA). (G) Fold change of metabolites from T cells differentiated in Th1 and Th17 conditions in the presence of CB839 relative to vehicle by mass spectrometry over 5 days. (H) ³H-2-deoxyglucose uptake in Th1- and Th17-skewed T cells at day 3 (left) and day 5 (right) (Student's t test). (I) Extracellular acidification rate (ECAR) of Th1- and Th17-skewed T cells at day 5 as in (H). (J) Fold change of Tbet (Th1) or RORyt (Th17) protein levels and (K) cell size in CB839-treated cells normalized to vehicle from same experiment as (G).

Also see Figure S4.

Author Manuscript

Author Manuscript

Author Manuscript

Author Manuscript

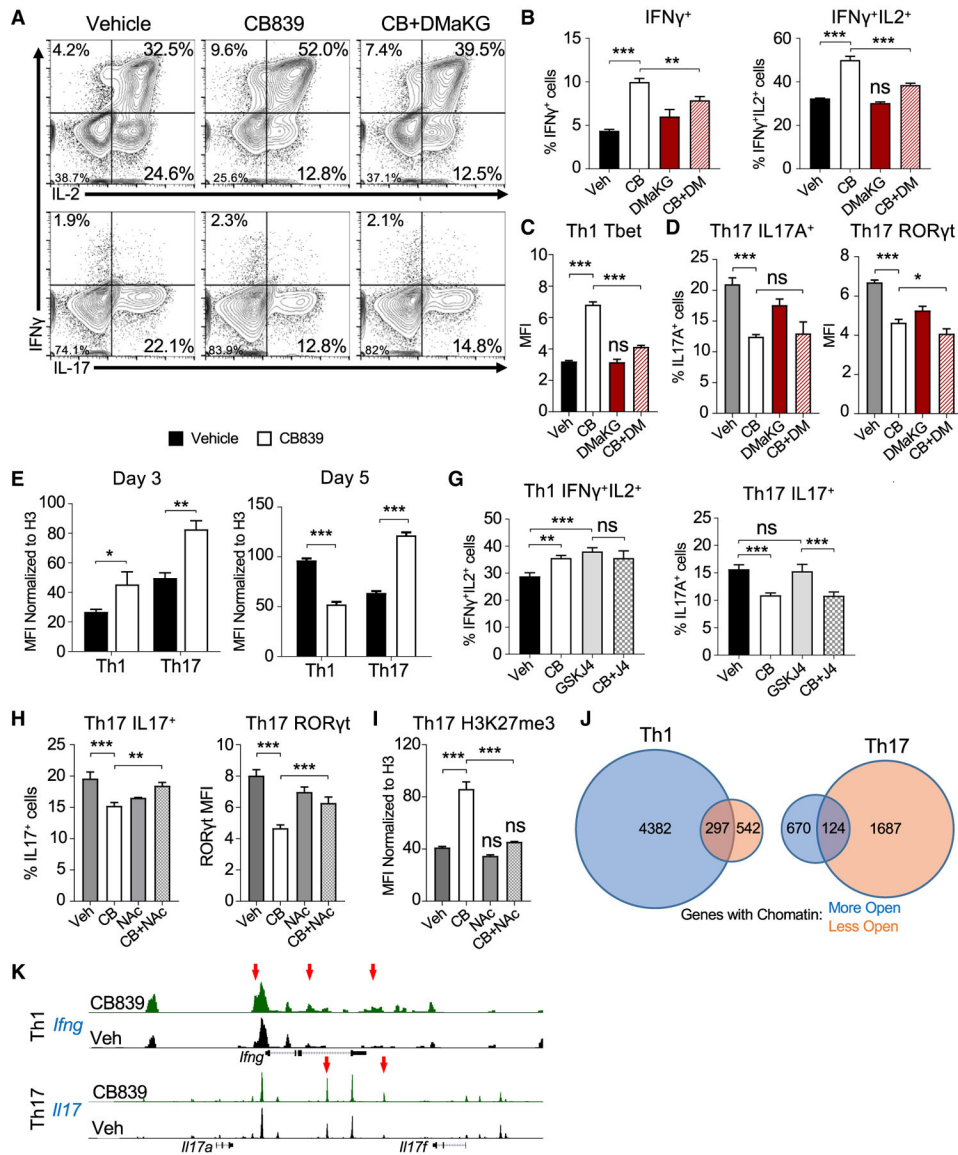


Figure 5. Th17 and Th1 Cells Differentially Rely on GLS-Mediated ROS Neutralization and Production of α -Ketoglutarate to Maintain Chromatin

(A–D) WT CD4⁺ T cells differentiated in Th1 or Th17 conditions in the presence of vehicle or CB839 over 5 days. (A) Cytokine production in Th1 (top)- and Th17 (bottom)-skewing conditions dosed as indicated. (B) Average IFN γ ⁺ only producers (left) and average IFN γ ⁺IL2⁺ producers (right) as in (A). (C) Average protein expression of Tbet as in (A). (D) Average IL-17A producers in Th17-skewing media (left) and average ROR γ t expression (right) (one-way ANOVA).

(E and F) Global H3K27 trimethylation normalized to total H3 by flow cytometry. (E) Average H3K27 trimethylation expression at day 3. (F) Same as (E), but at day 5 (Student’s t test).

(G) Average cytokine producers of skewed CD4⁺ T cells in the presence of CB839, JMJD3-inhibitor GSKJ4, or CB839+GSKJ4 (CB+J4) at day 5 (one-way ANOVA).

(H and I) WT CD4⁺ T cells differentiated in Th17 conditions as indicated. (H) Percent IL17A⁺ producers (left) and protein expression of ROR γ t (right). (I) Average expression of H3K27me3 normalized to total H3 as in (H) (one-way ANOVA).

(J) Number of loci with more (blue circles) and less accessible (orange circles) chromatin peaks with CB839 as determined by ATAC-seq.

(K) Example ATAC-seq traces of IFN γ in Th1 and IL17 gene locus in Th17-skewing conditions.

Also see Figure S5.

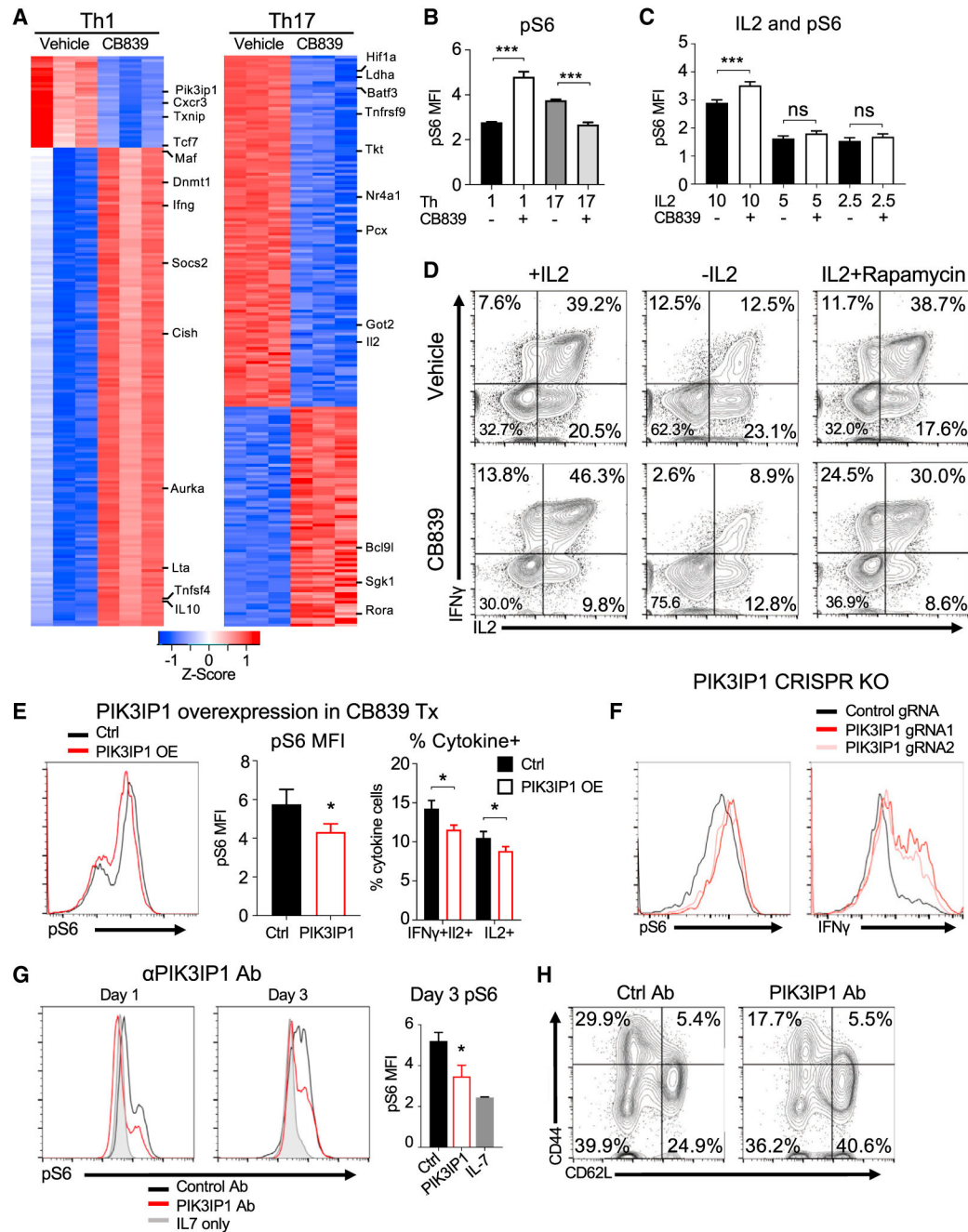


Figure 6. GLS Inhibition Alters Gene Expression to Sensitize Th1 Cells to IL2 Activation of mTORC1

(A) Top 200 modified genes from RNA-seq compared to vehicle ($\text{Log}_2\text{Fold} > 0.5$, $p < 0.05$) in Th1 (left) and Th17 (right).

(B and C) Phospho-S6 expression on day 5 in Th1 and Th17 conditions as indicated with or without CB839 or IL2 at concentrations shown (ng/mL) at day 3 (Student's *t* test).

(D) Cytokine production in Th1-skewing conditions in the presence of vehicle (top) or CB839 (bottom) after 5 days, under no IL2 conditions or with IL2 + mTOR inhibitor rapamycin added on day 3.

(E) Phospho-S6 protein expression (left), average pS6 MFI (middle), percent IFN γ ⁺IL2⁺ or IL2⁺ cells (right) in CD4 T cells in Th1-skewing conditions and infected with control- or PIK3IP1-expressing retrovirus with CB839-treatment. (middle, Student's t test; right, two-way ANOVA).

(F) Protein expression of phospho-S6 (left) and IFN γ (right) in activated Cas9-transgenic CD4⁺ T cells transduced with retrovirus-containing control guide RNA or guide RNAs targeting PIK3IP1.

(G and H) Wild-type CD4⁺ T cells activated and treated with PIK3IP1 antibody or IgG control antibody over 3 days. Protein expression of phospho-S6 (left) and average MFI of pS6 (right, one-way ANOVA). (H) Protein expression of activation markers of control or PIK3IP1 antibody-treated T cells upon stimulation (no CB839). Also see Figure S6 and Table S2.

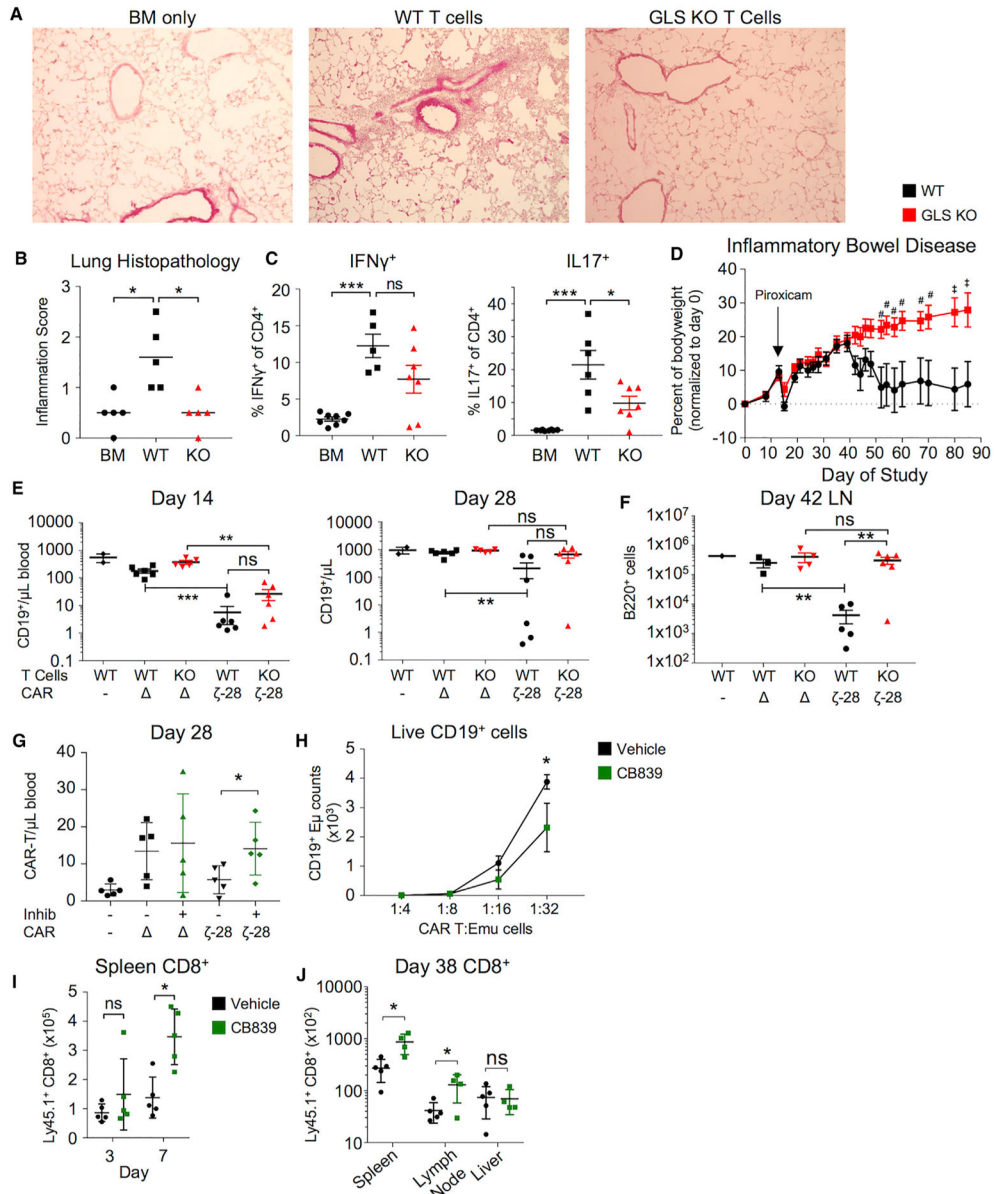


Figure 7. GLS Is Essential for T Cell-Mediated Inflammation, but Transient Inhibition Can Augment T Cell Responses

(A–C) Airway inflammation in cGvHD following transfer of WT or GLS KO T cells. (A) Hematoxylin- and eosin-stained lung sections focusing on bronchioles.

(B) Average histopathological scores from sections from (A) (unpaired t test). (C) Percent cytokine producers from peripheral lymph node cells stimulated with PMA/ionomycin for 5 hr from GvHD mice (BM, n = 8; WT, n = 5; KO, n = 7; unpaired t test).

(D) Bodyweights from T cell adoptive transfer inflammatory bowel disease (IBD) model in which RAG1 KO mice injected with WT and GLS KO naive CD4⁺ T cells and induced for IBD with piroxicam (#p < 0.05, ‡p < 0.01, two-way ANOVA; WT, n = 6; GLS KO, n = 8; data presented as SEM).

(E) CD19⁺ cells in blood at Day 14 and Day 28. (F) B220⁺ cells in Day 42 LN. (G) CAR-T/7/ μ L blood at Day 28. (H) Live CD19⁺ cells and CD19⁺ E μ counts at Day 28. (I) Spleen CD8⁺ cells at Day 3 and Day 7. (J) CD8⁺ cells in Spleen, Lymph Node, and Liver at Day 38.

(E and F) T cells from WT and GLS KO infected to express CAR T cell constructs and injected into recipient mice. CAR- no infection; Δ , m19-delta- ζ ; 28- ζ , m19-28- ζ . (E) CD19⁺ B cells per μ L of blood at day 14 (left) and day 28 (right). (F) Same as in (E), but at day 42 (one-way ANOVA).

(G) CAR T cell numbers on day 28 following transfer of CAR T cells treated with vehicle or CB839 prior to transfer to recipient mice (WT no CAR, n = 2 animals; all others, n = 5–6 animals; one-way ANOVA).

(H) Number of CD19⁺ E μ -Myc lymphoma cells after 48 hr culture with indicated ratios of CAR T cells (Student's t test).

(I) Counts of total CD8⁺ cells in response to hgp100_{25–33}-expressing vaccinia virus collected from tail vein after indicated time (two-way ANOVA).

(J) Counts of total CD8⁺ T cells in spleen (left) and lymph node (right) after 38 days and re-challenge with hgp100_{25–33}-expressing vaccinia virus (Vehicle, n = 5 animals; GLS inhibitor, n = 4 animals; two-way ANOVA).

Also see Figure S7.

KEY RESOURCES TABLE

REAGENT or RESOURCE	SOURCE	IDENTIFIER
Antibodies		
Anti-IFN γ functional	ThermoFisher	Cat#116-7311-38; RRID:AB_2637490
Anti-IL4 functional	ThermoFisher	Cat#16-7041-95; RRID:AB_2573101
Anti-CD3 functional	ThermoFisher	Cat#16-0038-85; RRID:AB_468857
Anti-CD28 functional	ThermoFisher	Cat#16-0289-85; RRID:AB_468927
Anti-PIK3IP1	ProteinTech	Cat#16826-1-AP; RRID:AB_2163333
Anti-GLS1 antibody	GeneTex	Cat#GTX81012; RRID:AB_11162809
Anti-IFN γ APC	BD	Cat#554413; RRID:AB_398551
Anti-IL17A PE	ThermoFisher	Cat#12-7177-81; RRID:AB_763582
Anti-IL2 PE	BD	Cat#554428; RRID:AB_395386
Anti-CD4 e450	ThermoFisher	Cat#48-0041-82; RRID:AB_10718983
Anti-CD8BV510	BD	Cat#563068; RRID:AB_2687548
Anti-Thy1.1 e450	ThermoFisher	Cat#48-0900-82; RRID:AB_1272254
Anti-CD25 e450	ThermoFisher	Cat#48-0251-82; RRID:AB_10671550
Anti-CD44 PECy5	ThermoFisher	Cat#15-0441-82; RRID:AB_468749
Anti-CD62L APC	ThermoFisher	Cat#17-0621-82; RRID:AB_469410
Anti-FOXP3 PE	ThermoFisher	Cat#12-5773-82; RRID:AB_465936
Anti-Tbet PE	ThermoFisher	Cat#12-5825-82; RRID:AB_925761
Anti-Tbet PECy7	ThermoFisher	Cat#25-5825-82; RRID:AB_11042699
Anti-RORYt APC	ThermoFisher	Cat#12-6988-82; RRID:AB_1834470
Anti-CD19APC	Biologend	Cat#115512; RRID:AB_313647
Anti-CD45RB	Biologend	Cat#103320; RRID:AB_2565229
Anti-pS6 PE	Cell Signaling Technology	Cat#5316S; RRID:AB_10694989
Anti-c-Myc PE	Cell Signaling Technology	Cat#14819S
Anti-H3K27me3 af647	Cell Signaling Technology	Cat#12158S
Anti-H3K4me3 af647	Cell Signaling Technology	Cat#12064S
Anti-H3 total protein af647	Cell Signaling Technology	Cat#12230S
Isotype PE control	ThermoFisher	Cat#12-4714-42; RRID:AB_1944423
APC-conjugated Tetramers	(Moon et al., 2007)	N/A

REAGENT or RESOURCE	SOURCE	IDENTIFIER
Chemicals, Peptides, and Recombinant Proteins		
Recombinant Mouse IL2	ThermoFisher	Cat#14-8021-64
Recombinant Mouse IL-7	Peptotech	Cat#217-17
Recombinant IL12p70	ThermoFisher	Cat#14-8121-62
Recombinant TGFβ	R&D systems	Cat#100-B-001
Recombinant IL6	ThermoFisher	Cat#14-8061-80
2-deoxyglucose	Sigma-Aldrich	Cat#D6134; CAS 154-17-6
Dimethyl 2-oxoglutarate	Sigma-Aldrich	Cat#349631; CAS 13192-04-6
D-Glucose(U-13C6)	Cambridge Isotope Labs	Cat#CLM-1396-1
Deoxy-D-glucose 2-[1,2,3H(N)]	Perkin Elmer	Cat#NET549001MC
phase Dinonyl phthalate	Sigma-Aldrich	Cat#80151
Dow Corning Silicon 550 oil	Motion Industries, INC	Cat#784198
Phoretin	Millipore	Cat#524488; CAS 60-82-2
GSKJ4	Selleckchem	Cat#S7070
UK5099	Sigma-Aldrich	Cat#PZ0160; CAS 56396-35-1
CB839	Calithera Biosciences	N/A
Gls1 inhibitor III	Millipore	Cat# 533717; CAS 1439399-58-2
Hgp100/ ²⁵⁻³³ KVPRNQDWL	(Gattinoni et al., 2009)	N/A
Gp100-W vaccinia virus vector	(Overwijk et al., 1998)	N/A
2W peptide EAWGALANWAVDSA	GenScript	N/A
Rapamycin	Sigma Aldrich	Cat#553210
GolgiPlug	BD	Cat#555029
PMA	Sigma Aldrich	Cat#P8139
Ionomycin	Sigma Aldrich	Cat#IO634
Cell Trace Violet	Invitrogen	Cat#c34557
ACK Lysing Buffer	VWR	Cat#10-548E
Cyclophosphamide	Sigma Aldrich	Cat#C0768
Complete Freund's Adjuvant	Sigma Aldrich	Cat#F5881
Critical Commercial Assays		
Genomic DNA clean & concentrator	Zymo Research	Cat#D4011
Nextera DNA prep kit	Illumina	Cat#FC-121-1030

REAGENT or RESOURCE	SOURCE	IDENTIFIER
Nextera index kit	Illumina	Cat#FC-121-1011
CD4+ isolation kit	Miltenyi	Cat#130-104-454
CD8+ isolation kit	Miltenyi	Cat#130-095-236
Pan T cell isolation kit	Miltenyi	Cat#130-095-130
Fix/pern kit	ThermoFisher	Cat#88-8824-00
Fixation/permeabilization kit	BD	Cat#554715
NEBNext High-fidelity 2x PCR mix	New England Biolabs	Cat#M0541
RNeasy Mini Kit	QIAGEN	Cat#74104
NEBNext Ultra RNA Library Kit	New England Biolabs	Cat#E7530
XF Mito Stress test kit	Agilent	Cat#103015-100
KAPA express Extraction Kit	KAPA	Cat#KK5121
Deposited Data		
RNA Seq data	This paper	GEO: GSE112244; https://www.ncbi.nlm.nih.gov/geo/query/acc.cgi?acc=GSE112244
ATAC Seq data	This paper	ArrayExpress: E-MTAB-6648 https://www.ebi.ac.uk/arrayexpress/experiments/E-MTAB-6648/
Experimental Models: Cell Lines		
CD19+ Eμ-ALL01 cells (Emu)	(Davita et al., 2013)	N/A
Plat-E retroviral packaging cell line	Cell Biolabs	Cat#RV-101
E. Coli LPS	Sigma	Cat#L4391
Dust Mite Antigen	Greer	Cat#XPB70D3A2.5
Experimental Models: Organisms/Strains		
Mouse: GLS KO: GLS ^{fl/fl} CD4-CRE mice	This paper	N/A
Mouse: pme1 Tg mouse: B6.Cg-Thy1a/Cy Tg(TeraTerb)8Rest/J	(Sukumar et al., 2013)	RRID: IMSR_JAX:005023
Mouse: C57BL6	Jackson Labs	RRID: IMSR_JAX:000664
Mouse: RAG1 KO	Jackson Labs	RRID: IMSR_JAX:002216
Mouse: CAS9	Jackson Labs	RRID: IMSR_JAX:024858
Oligonucleotides		
GLS KO Forward ACGAGAAAGTGGAGATCG	This paper	N/A
GLS KO reverse GCCTTCTGGAAAACA	This paper	N/A
PIK3IP1 guide RNA 1 AGACCGGCGTCCCTGAAAAG	This paper	N/A
PIK3IP1 guide RNA 2 TCGTGGGCTACACTTACAAG	This paper	N/A
Recombinant DNA		

REAGENT or RESOURCE	SOURCE	IDENTIFIER
Plasmid MSCV-IRES-Thy1.1	(Wu et al., 2006)	Addgene Cat#17442
Plasmid MSCV-Pik3ip1-IRES-Thy1.1	(Wei et al., 2016)	N/A
Plasmid pMx-U6-empty-GFP	(Toffalini et al., 2009)	N/A
Plasmid pMx-U6-PIK3IP1-gRNA1-GFP	This paper	N/A
Plasmid pMx-U6-PIK3IP1-gRNA2-GFP	This paper	N/A
Software and Algorithms		
Flowjo version V10	Flowjo	https://www.flowjo.com ; RRID: SCRJD08520
GraphPad Prism v6.0	GraphPad Software	https://www.graphpad.com ; RRID: SCR_002798
R statistical software	R Foundation	https://www.r-project.org/
STAR software	(Mudge and Harrow, 2015)	https://github.com/alexdobin/STAR
SAMtools	(Li et al., 2009)	http://samtools.sourceforge.net/
featureCounts	(Liao et al., 2014)	http://subread.sourceforge.net/
DESeq2 Sequencing software	(Love et al., 2014)	N/A